

SET SCREW BREAK-OFF STUDY IN SPINAL NEUROSURGERY

by

Ganesh Gautham Aswapathi Ramesh

B.E., People's Education Society Institute of Technology, 2003

A Thesis

**Submitted in Partial Fulfillment of the Requirements for the
Degree of Master of Science**

**Department of Mechanical Engineering and Energy Processes
In the Graduate School
Southern Illinois University Carbondale
August 2009**

UMI Number: 1469284

INFORMATION TO USERS

The quality of this reproduction is dependent upon the quality of the copy submitted. Broken or indistinct print, colored or poor quality illustrations and photographs, print bleed-through, substandard margins, and improper alignment can adversely affect reproduction.

In the unlikely event that the author did not send a complete manuscript and there are missing pages, these will be noted. Also, if unauthorized copyright material had to be removed, a note will indicate the deletion.

UMI[®]

UMI Microform 1469284
Copyright 2009 by ProQuest LLC
All rights reserved. This microform edition is protected against
unauthorized copying under Title 17, United States Code.

ProQuest LLC
789 East Eisenhower Parkway
P.O. Box 1346
Ann Arbor, MI 48106-1346

THESIS APPROVAL

SET SCREW BREAK-OFF STUDY IN SPINAL NEUROSURGERY

By

Ganesh Gautham Aswapathi Ramesh

**A Thesis Submitted in Partial
Fulfillment of the Requirements
for the Degree of
Master of Science
in the field of Mechanical Engineering**

Approved by:

Dr. T. C. Chu, Chair

Dr. A. M. Mahajan

Dr. J. Don

Dr. B. Schwartz

**Graduate School
Southern Illinois University Carbondale
February 26th, 2009**

ABSTRACT

AN ABSTRACT ON THE THESIS OF

GANESH GAUTHAM ASWAPATHI RAMESH, for the Master of Science degree in Mechanical Engineering, presented on February 26th, 2009, at Southern Illinois University Carbondale.

TITLE: SET SCREW BREAK-OFF STUDY IN SPINAL NEUROSURGERY

MAJOR PROFESSOR: Dr. T. C. Chu

This thesis describes the measurement of high g-forces, in the range of 400-800g's occurring in a spinal construct during the breaking of the set-screw head using a manual torquing instrument. The measurements were validated using a high speed camera. The design torque (11 N-m) required for breaking the set-screw was compared with the torque calculated from the distortion energy theory for material fracture (9.9 N-m) and an actual measurement using a torque wrench (11.3 N-m). A comparison between the manual and powered instruments showed a 27.68% reduction in g-forces and a 36.42% reduction in die-down time while using the powered instrument. 8.52% less energy was felt on the adjoining screw. The consistency in the powered instrument is higher because the standard deviation using the manual instrument is 8.46, compared to the powered instrument which was 8.31. Also 25g's was recorded on the surgeon's wrist and elbow. Based on previous work done, the external work done by the surgeon was about 60-120 KJ. The onset of fatigue was apparent in consecutive break events as illustrated by the change in EMG parameters over time.

DEDICATION

To my parents, for all of their support and guidance throughout my life.

ACKNOWLEDGMENTS

This work would not have been possible without the support and encouragement of my advisor, Dr. Tsuchin Chu, under whose supervision I chose this topic and began the thesis. He has been abundantly helpful in numerous ways – academically and otherwise with his constructive criticism, constant encouragement and unstinted support. Without him, I would have been lost. I am thankful to him for his patience, guidance and all kinds of support he has given me generously. His words of advice will be with me for the rest of my life.

My thanks and appreciation goes to my thesis committee members, Dr. Ajay Mahajan, Dr. Jarlen Don and Dr. Bradley Schwartz for their continuous support, guidance and invaluable advice. In particular, I would like to thank Dr. Mahajan for providing me with an opportunity to work on this project. This project would not have been completed without his assistance and guidance during the course of this entire project.

I am greatly indebted to the Chair and Staff of the Department of Mechanical Engineering and Energy Processes for supporting me financially throughout my graduate studies.

I also wish to thank my colleagues and friends Rick Miller, Yi-cheng Pan and Ryan Stickle for being tolerant with me. This thesis would not be possible without their continual support, constant reminders, and assistance in problem solving. I am grateful to them for helping me in preparing the test setup, testing,

analyzing and in completing the project. To them, I owe a lot. I will cherish their friendship and the time I spent with them.

I would like to thank all my friends who helped me get through two years of graduate school. In particular, I would like to thank them for giving me constant pointers, support and letting me take my frustrations out on them. I truly value their friendship.

Finally, I would like to thank my family members for their unconditional love and support.

TABLE OF CONTENTS

ABSTRACT	i
DEDICATION	ii
ACKNOWLEDGMENTS	iii
LIST OF TABLES	viii
TABLE OF FIGURES	ix
CHAPTER 1 - INTRODUCTION	1
1.1 Literature Review	3
1.1.1 The Human Spine	3
1.1.2 Anatomy of the Spinal Cord	4
1.1.3 The Intervertebral Disc	6
1.1.4 Pedicles in the Spine	7
1.1.5 Function of the Human Spine	8
1.1.6 Function of the Intervertebral Disc	8
1.1.7 Diseases Affecting the Human Spine	9
1.1.8 Pedicle Screws and Fixation Systems	11
1.1.9 Spinal Construct	14
1.2 Flow of Work	15
CHAPTER 2 – G-FORCE AND TORQUE MEASUREMENTS	16

2.1 G-Force Measurement Tests and Validation.....	17
2.1.1 G-Force Accelerometer Test Set-up	18
2.1.2 Fixtures	18
2.1.3 Bench Results for Accelerometer Tests.....	21
2.1.4 Extended G-force Measurements Tests	22
2.1.5 Extended G-force Test Set-up	23
2.1.6 Test Results	25
2.1.7 High Speed Camera Test Set-up and Results	28
2.1.8 Validation Using High Speed Camera.....	30
2.2 Measurement of Torque and Results	36
2.2.1 Distortion Energy Theory (DET)	36
2.2.2 Fully Plastic Torque (FPT)	39
2.2.3 Torque Measurement Using a Torque Wrench	39
2.3 Results – Comparison of G-Force and Torque.....	41
2.4 Summary on G-Force and Torque Measurements	42
CHAPTER 3 – NEUROSURGICAL POWERED AND MANUAL	
TORQUING INSTRUMENT PERFORMANCE COMPARISON	43
3.1 Tru-Trainer and Cadaver Laboratory Test Set-up	45
3.2 Tru-Trainer and Cadaver Lab Data Analysis.....	47
3.2.1 3Dx Station (Manual/Powered Instrument Test Analysis)....	47
3.2.2 Data obtained from Surgeons	53

3.3 Data Comparison for Manual and Powered Prototype	58
3.4 Summary for Manual / Powered Instruments Comparison	61
CHAPTER 4 – ONSET OF FATIGUE IN A SURGEON BASED ON BENCH RESULTS OF G-FORCE MEASUREMENTS	63
4.1 EMG Test Set-up and Data Collection	65
4.2 Onset of Fatigue	68
4.3 EMG Data Analysis	71
4.4 Summary on Onset of Fatigue Study	76
CHAPTER 5 – CONCLUSIONS AND RECOMMENDATIONS.....	77
REFERENCES	82
APPENDICES	85
VITA	86

LIST OF TABLES

Table 1: Multi-level Construct Test Data	26
Table 2: Inner and Outer Diameter values	37
Table 3: Comparison of G-Force Values	41
Table 4: Comparison of Torque Values	41
Table 5: Performance Data by Surgeon 1 using a Tru-trainer	53
Table 6: Performance Data by Surgeon 1 using a Cadaver	54
Table 7: Performance Data by Surgeon 2 using a Tru-trainer	54
Table 8: Performance Data by Surgeon 2 using a Cadaver	55
Table 9: Performance Data by Surgeon 3 using a Tru-trainer	55
Table 10: Performance Data by Surgeon 3 using a Cadaver	56
Table 11: Performance Data by Surgeon 4 using a Tru-trainer	56
Table 12: Performance Data by Surgeon 4 using a Cadaver	57
Table 13: Performance Data by Surgeon 5 using a Tru-trainer	57
Table 14: Performance Data by Surgeon 5 using a Cadaver	58
Table 15: Calculated Percentage Reduction for Cadaver Data.....	59
Table 16: Percentage Reduction using the powered instrument	60
Table 17: Standard Deviation for the Work Done	61
Table 18: Components of Titanium Alloy Ti-6Al-4V [51]	1

TABLE OF FIGURES

Figure 1: Typical Spinal Column.....	4
Figure 2: Spinal Segment. [6]	6
Figure 3: Overhead view of the Intervertebral Disk. [6].....	7
Figure 4: Pedicle Screw Fixation System [Courtesy: Medtronic].....	12
Figure 5: Smaller Spinal Construct.....	14
Figure 6: Larger Spinal Construct.....	14
Figure 7: Pedicle Screw Implant.....	17
Figure 8: Torquing Instruments	17
Figure 9: Laboratory Set-up.....	18
Figure 10: Fixture 1 for Accelerometer	19
Figure 11: Installation of the fixture and accelerometer	20
Figure 12: Results of Test 1 showing 500g acceleration	21
Figure 13: Results of Test 2 showing 600g acceleration	21
Figure 14: Test run that shows almost 800g acceleration	22
Figure 15: Accelerometer placed on smaller multi-level construct	24
Figure 16: Set-up for multi-level construct test	24
Figure 17: Torquing of the set screw.....	25
Figure 18: Maximum g-forces at different locations.....	26

Figure 19: Average of the maximum g-forces.....	27
Figure 20: Vision Research.....	28
Figure 21: Motion Engineering.....	28
Figure 22: Olympus i-speed 3.....	28
Figure 23: Vision Research Camera Test Set-up.....	29
Figure 24: Motion Engineering Camera Test Set-up.....	29
Figure 25: Olympus i-speed 3 Camera Test Set-up.....	29
Figure 26: Track Eye Motion Analysis (TEMA) software [31].....	30
Figure 27: Two points marked on the construct.....	31
Figure 28: Path of the two points marked in red and blue.....	31
Figure 29: X direction Displacement from TEMA.....	32
Figure 30: Y Direction displacement from TEMA.....	33
Figure 31: X Direction Velocity from TEMA.....	33
Figure 32: Y Direction Velocity from TEMA.....	34
Figure 33: X Direction Acceleration from TEMA.....	34
Figure 34: Y Direction Acceleration from TEMA.....	35
Figure 35: X direction acceleration (accelerometer).....	35
Figure 36: Set Screw heads in foam with measurement scale.....	36
Figure 37: Inner, Outer Diameter and Stress Distribution in a cylinder.....	38

Figure 38: Torque Wrench from Craftsman® [35].....	40
Figure 39: Manual Torquing Instruments	45
Figure 40: Tru – Trainer Laboratory Set-up.....	46
Figure 41: Cadaver Laboratory Set-up	46
Figure 42: Plots of Accelerometer readings against time.....	49
Figure 43: Trendlines of the accelerometer readings against time.....	49
Figure 44: Plot of RMS value and Trend line.....	50
Figure 45: Spline used to identify area under curve	50
Figure 46: Plots of Accelerometer readings against time.....	51
Figure 47: Trendlines of the accelerometer readings against time.....	51
Figure 48: Plot of RMS value and Trend line.....	52
Figure 49: Spline used to identify area under curve	52
Figure 50: Cadaver Lab Results Summary.....	62
Figure 51: EMG Data Acquisition and Monitoring System.....	65
Figure 52: EMG Test Laboratory Set-up	66
Figure 53: EMG Data Recording.....	67
Figure 54: Surface EMG of the Event.....	68
Figure 55: Median Frequency Content of the EMG Density Spectrum	69
Figure 56: Integrated EMG from forearm muscles	70

Figure 57: EMG Data Series 1	71
Figure 58: Normalized EMG Data Series 1	72
Figure 59: EMG Data Series 2	72
Figure 60: Normalized EMG Data Series 2	73
Figure 61: EMG Data Series 3	73
Figure 62: Normalized EMG Data Series 3	74
Figure 63: EMG Data Series 4	74
Figure 64: Normalized EMG Data Series 4	75
Figure 65: Probability Chart showing Fatigability	75
Figure 66: Performance Comparison of the 5 Surgeons	79

CHAPTER 1 - INTRODUCTION

The main objective of a pedicular fixation system is to correct deformity and to stabilize the spine. The purpose for choosing the pedicle as the place for screw fixation to achieve these goals arises from anatomic as well as from biomechanical factors. The pedicle is considered to be the strongest part through which the vertebra is accessible and it is large enough to fix the screws. The main purpose of this research was to test a multilevel spinal construct and determine g-forces and torques acting on the spine during set-screw break-off with the use of torquing and other instruments. This study also focused on the determining of g-forces on successive screws as well as the surrounding medium. In this study, the torque was determined by machine design theories and was compared with the actual design value. Using the results obtained from the g-force measurements, a comparative study was made between manual and powered torquing instruments. This research study also focused on determination of the external work done by the neurosurgeon in using the manual torquing instrument; calculate the metabolic rate and eventually the fatigability involved. This study included investigating the fatigability in a surgeon while using the manual torquing instrument. The energy expended by the surgeon during breaking off eventually leading to the onset of fatigue was also determined. Effect of the torquing of the set screws on the spinal construct in terms of work done was investigated.

Pedicle screws are commonly used implants for spinal stabilization with a widespread use. They have become increasingly popular worldwide. A variety of pedicle screw systems are being developed every day. Pedicle fixation and spinal fusion have been associated with extensive blood loss, lengthy hospital stays, and significant cost. Of the many types of pedicle screws available, top-loading pedicle screws have been used in this study. These top-loading screws were used on the spinal construct and the set screws were torqued off using the manual torquing instruments available.

Though studies are available on the axial pull-out strengths of screws, no studies have been reported so far which have considered the torque developed, g-forces acting on the surgeon and the onset of fatigue during breaking off of multiple set screws [1]. This study is significant because it examined the effects of different variables during break off of the set screws but it represented an idealized clinical situation. The focus was on measuring the g-forces and torque on the spinal construct during breaking off. Bench tests were performed to determine the g-forces being developed in the wrists and elbow of the surgeon during this event. Studies were conducted to determine the energy expended by the surgeon eventually leading to the onset of fatigue.

1.1 Literature Review

1.1.1 The Human Spine

The central nervous system consists of the brain and the spinal cord protected by three membranous connective tissue coverings called as the meninges. They are called the dura mater, the arachnoid membrane, and the pia mater. The human spine is a unique flexible structure. The spine is composed of living bone, cartilaginous elements, joints, spinal cord, nerve roots, ligaments, tendons, muscles, and a vascular system. The spinal column also called the vertebral column consists of vertebrae and intervertebral disk stacked in alternate layers [2]. The spinal cord consists of a core of grey matter (sensory) surrounded by a thicker section of white matter (motor). The upper and lower wings of grey matter refer to posterior and anterior horns. The neurons with large cell bodies in the anterior horns give rise to motor fibers that come out through spinal nerves to skeletal muscle. The neurons in the grey matter of the spinal cord connect with other neurons to form a nerve pathway. The white matter of the spinal cord has myelinated nerve fibers called nerve tracts. These fibers provide a system of communication between the brain and body areas outside the nervous system. The tracts that send impulses from the body to the brain with sensory inputs are called ascending tracts and the tracts that send motor impulses from the brain to muscles and glands are called as the descending tracts [3].

1.1.2 Anatomy of the Spinal Cord

The spinal cord is located inside the vertebral canal and is made up of three groups of vertebrae called as Lumbar, Thoracic and Cervical [3]. Figure 1 is a typical model of the spinal column.

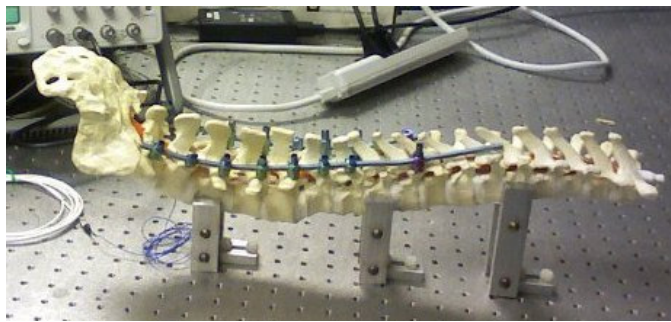


Figure 1: Typical Spinal Column.

There are 5 lumbar vertebrae in the lower back. They support the most weight and hence are stronger. There are 12 thoracic vertebrae in the middle (chest area). They downwards, and have facets on the sides of their bodies that join with ribs. Beginning with the third thoracic vertebra and moving down, the bodies of these bones increase in size. There are seven cervical vertebrae that form the bony axis of the neck. These are the smallest of the vertebrae and their bone tissues are denser than others. The transverse processes of the cervical vertebrae have transverse foramina, which serve as passageways for arteries leading to the brain. The spinous processes of the second through the fifth cervical vertebrae are uniquely forked and provide attachments for various

muscles. The first vertebra known as atlas supports and balances the head. It has practically no body or spine and appears as a bony ring with two transverse processes. The second vertebra is the axis.

The spinal cord consisting of nerve fibers form the central nervous system along with the brain. It is enclosed and protected by the bony vertebral column and surrounded by the Cerebral Spinal Fluid (CSF). The main function of the spinal cord is transmission of neural inputs between the periphery nervous system and the brain. The nerves comprise of the sensory nerve roots and the motor roots. The spinal nerves pass out through a hole in each of the vertebrae to carry the information from the spinal cord to the rest of the body, and from the body to the brain. The spinal nerves continue as a bundle of nerves called the cauda equine after the end of the spinal cord. The spinal nerves are named and numbered according to the place that they enter the cord and the place where they emerge from the cord [4]. The main groups of spinal nerves are [5]:

- a. Cervical Nerves 'C' – movement and feeling to the arms, neck and upper trunk.
- b. Thoracic Nerves 'T' – Supply the trunk and abdomen.
- c. Lumbar Nerves "L" & Sacral Nerves 'S' – legs, bladder, bowel & sexual organs.

1.1.3 The Intervertebral Disc

The intervertebral discs consist of the nucleus pulposus, annulus fibrosus and vertebral end-plates. A typical vertebra has a drum-shaped body called as the centrum which forms a thick, anterior portion of the bone as shown in Figure 2. The intervertebral disks, separate the vertebrae. Each intervertebral disk is composed of a band of fibrous fibro cartilage known as the annulus fibrosus. The annulus fibrosus surrounds a gelatinous core called as the nucleus pulposus as shown in Figure 3. The bodies of adjacent vertebrae are joined on the front surfaces by anterior ligaments and on the back by posterior ligaments [7].

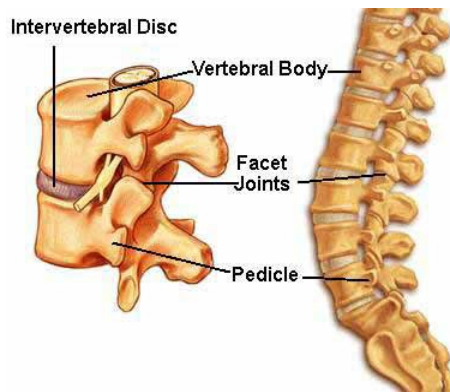


Figure 2: Spinal Segment. [6]

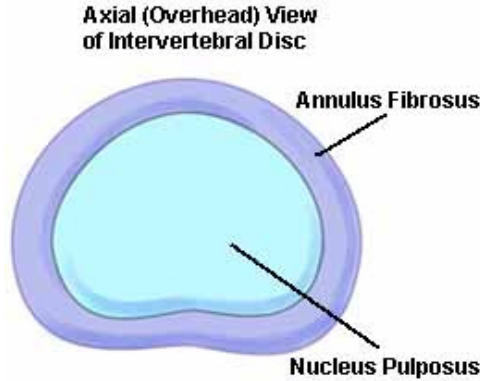


Figure 3: Overhead view of the Intervertebral Disc. [6]

1.1.4 Pedicles in the Spine

There are two short stalks called "pedicles" that project from the back of each body that form the sides of the vertebral foramen as shown in Figure 2. Two plates known as the laminae arise from the pedicles and fuse to become spinous process. The pedicles, laminae, and spinous process together form a bony vertebral arch around the vertebral opening, through which the spinal cord passes.

The transverse process projects laterally and toward the back, between the pedicles and laminae. Various ligaments and muscles are attached to the spinal process and the transverse process. Superior and inferior articulating processes project upward and downward from each vertebral arch. These processes bear cartilage-covered flat faces by which each vertebra is joined to the one above and the one below it. There are notches called intervertebral foramina on the surfaces of the vertebral pedicles that align to create openings.

These openings provide passageways for spinal nerves between joining vertebrae and connect to the spinal cord [7].

1.1.5 Function of the Human Spine

The human spine with a network of muscles, ligaments, bones, joints, cartilage and nerves work together to provide support and mobility to the body. The skeletal system supports the body against gravity, protects soft body parts, produce red blood cells, store inorganic calcium, and phosphorus salts. The Intervertebral disks act as shock absorbers [8]. The sensory nerve roots which enter the spinal cord transmit messages from the body to the brain while the motor nerves which exit the spinal cord control movement in the body. These sensory nerve roots and motor roots run through passageways, or foramina, between the bones of the spine. Irritation of the nerve roots occur when spinal structures are pinched or pressed against the roots [9].

1.1.6 Function of the Intervertebral Disc

The basis functions of the intervertebral disc include [10]:

- a. They hold the vertebrae of the spine together acting as a ligament
- b. They carry the downward weight or the axial load of the body acting as a shock absorber
- c. They act as pivot point, allowing the spine to bend, rotate and twist.

1.1.7 Diseases Affecting the Human Spine

Herniated Disk

Herniated disks occur when the nucleus pulposus is pushed out of the annulus. It is more commonly known as a slipped or ruptured disk. These occur during an early degeneration. This movement of the disk puts pressure on the spinal nerves causing severe pain. They are more common in the lumbar region of the spine, but also occur in the cervical part of the spine. They may be caused by an injury or excessive strain. Symptoms include pain, numbness or weakness. Most herniated disks do not require surgery. Surgery may be required if it cannot be treated by medication or therapy [11].

Spinal Stenosis

Spinal stenosis occurs due to a narrowing of spaces in the spine that result in pressure on the nerves. This causes severe pain, numbness, weakness, bowel and bladder problems, and in severe cases, partial paralysis. Though there are several forms of spinal stenosis, the most common occurs as a result of degeneration of the spine causing the narrowing of the spinal canal [12].

Spinal Deformity

Scoliosis, kyphosis and lordosis are some of the spinal deformities. Scoliosis is a spinal deformity where the spine is curved to the left or right. It usually occurs during childhood and may be corrected at that time. Kyphosis is a

deformity where the upper back curves forward, creating a hump like appearance on the back. Causes may be due to bad posture, fractures, or developmental problems. Lordosis is a spinal deformity that occurs when the lower back curves inward [13]. Minimally invasive surgery techniques help in overcoming some of these deformities.

Sciatica

Sciatica is the irritation or inflammation of the sciatic nerve, the largest nerve in the body. The sciatic nerve forms when several lumbar nerve roots join together in the pelvis. The most common cause of sciatica is pressure on one of the lumbar nerve roots that form the sciatic nerve. This is usually caused by a herniated disc or other spinal problems pushing on the nerve root. This causes shock or burning low back pain combined with pain through the buttock and down one leg to below the knee, occasionally reaching the foot [14].

Osteoporosis

Osteoporosis is a bone disease that is characterized by a decrease in bone density and strength [14].

1.1.8 Pedicle Screws and Fixation Systems

Brief History

The history of using internal fixation goes back to 1891 when Hadra used silver-wire internal fixation for the treatment of a cervical fracture-dislocation and tuberculous spondylitis [15]. King used facet screws for the treatment of degenerative lumbar conditions in 1948 [16]. Harrington and Tullos made the first attempt to implant pedicle screws through the isthmus of the pedicle [17]. Cotrel et al., Dick, Roy-Camille et al. and Louis continued the use of pedicle-screw internal fixation with clinical success in France and Switzerland in the 1980s [18-22]. Since the work of these early pioneers, pedicle screws have undergone many modifications in design and usage and have received widespread acceptance for spinal stabilization.

Pedicle Screw Fixation Systems

The pedicle screw is a type of bone screw, used in spinal surgery. They are called pedicle screws because they are implanted in the pedicles of the vertebrae. The screws hold plates or rods, allow the vertebrae to fuse and in the process immobilize the spine. These systems are used to treat fractures, degenerative arthritis, and reconstruction from tumors.

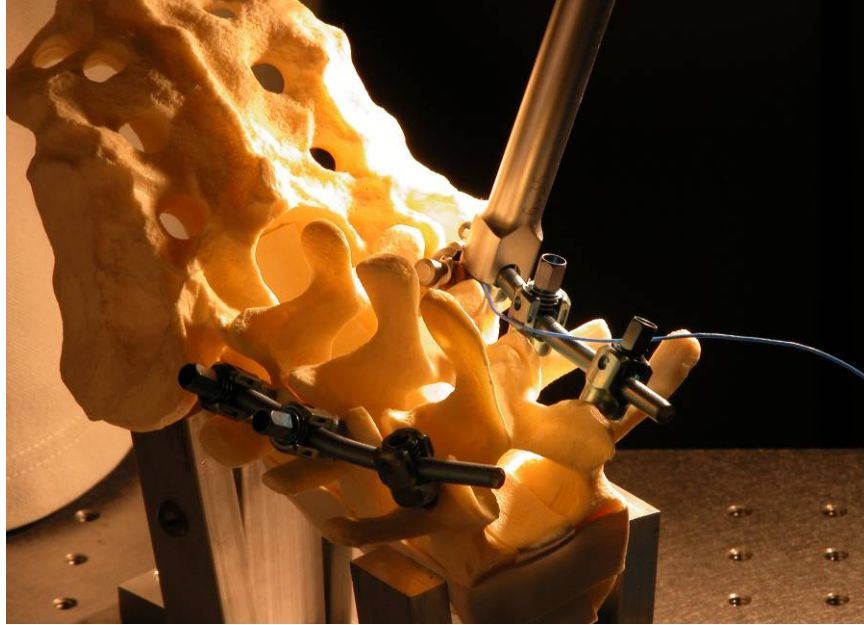


Figure 4: Pedicle Screw Fixation System [Courtesy: Medtronic]

Pedicle screw fixation systems are devices made out of multiple components. The components are made of either stainless or titanium steel. They consist of solid, grooved or slotted plates or rods that are interconnected longitudinally and anchored to adjacent vertebrae using bolts, hooks or screws [23]. The pedicle screw fixation system used in this study is shown in Figure 4.

Advantages and Disadvantages

Pedicle screws can bear a lot of weight. They have better biomechanical stability in normal bone. There are few complications with using pedicle screws. They require expertise on the part of the surgeon and can be expensive. There may be problems associated with the stiffness of the screws. As with any other surgery, there is potential for significant blood loss and increased risk of infection [26, 27].

Pedicle Screw Fixation Procedure

A suitable system is constructed using these components based on a patient's anatomical and physiological system. The method in which the pedicle screws are connected to the longitudinal support components is highly diversified and system-specific. Pedicle screws are inserted into channels that have been drilled through the cancellous central axis of each vertebral pedicle, during implantation of the spinal support system. The longitudinal supports usually cover two or more vertebrae. An anchoring screw is placed in both pedicles of each vertebra. Pedicle screw fixation systems are safe and effective. The successful use of pedicle screw fixation systems in spinal stabilization and in spinal fusion can be seen in patients with degenerative disc disease, thoracic fractures and lumbar tumors [23].

Implant Materials

Spinal Implant materials frequently used are stainless steel, commercially pure titanium and titanium-aluminium-vanadium alloy. The standardization of these materials is controlled by the American Society for Testing and Materials (ASTM). The composition of the alloys varies for different manufacturers [24]. Composition Ti-6Al-4V grade 5 alloy is given in Appendix B.

1.1.9 Spinal Construct

Two spinal constructs were used during this study, one smaller and one larger. The constructs are placed in a saw bone structure. The smaller spinal construct is a 3-level construct as shown in Figure 5 while the larger spine model has a multi-level construct as shown in Figure 6.

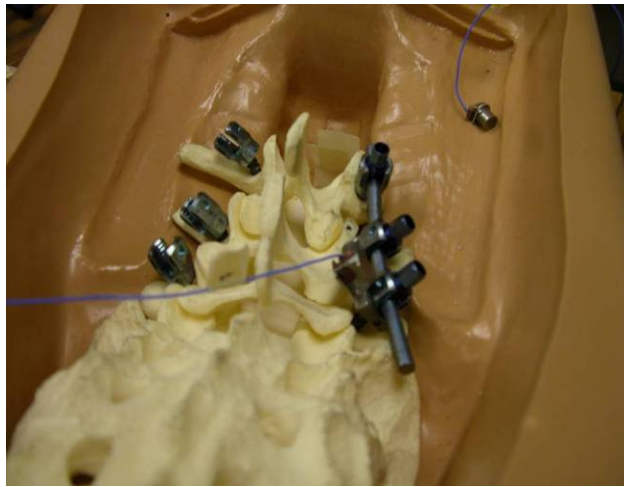


Figure 5: Smaller Spinal Construct

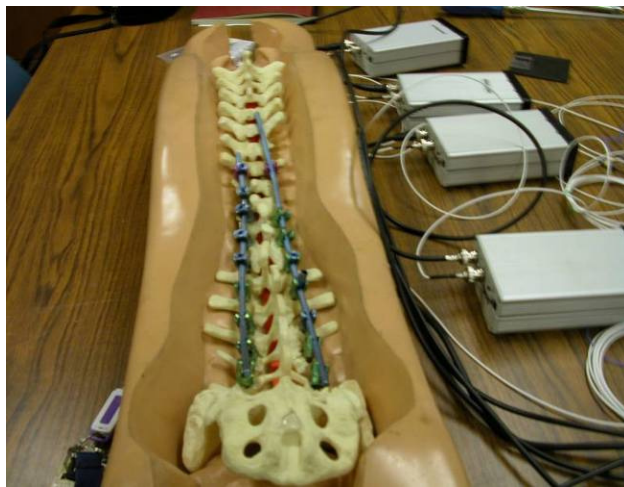


Figure 6: Larger Spinal Construct

1.2 Flow of Work

Chapter 1 provides the background information on the human spine. Anatomy, function and diseases of the spinal cord were discussed in that section. The chapter also gives brief information on the pedicles of the spine, pedicle screws, pedicle screw fixation systems and procedure. Chapter 2 describes the laboratory set-up and procedures followed for the measurement of G-forces and Torque. Background information is given on the instruments used in this process and material properties. A comparative study of neurosurgical powered and manual torquing instruments is given in Chapter 3. Using the bench results of G-force and torque measurements and the comparison of powered and manual torquing instruments, Chapter 4 discusses the onset of fatigue in surgeons during manual breaking-off of set screws. Chapter 5 describes the future work and the possibility of using biomaterials.

CHAPTER 2 – G-FORCE AND TORQUE MEASUREMENTS

The purpose of this study is to determine g-forces using modern instrumentation, and then validating the results using knowledge from materials engineering and machine design theories.

Moore, *et al.* conducted research studies to determine the pull-out strengths of the pedicle screws for comparison. They report that though there are many factors affecting the pedicle screw system, one of the main factors is the strength of their attachment to the spine [25]. Hirano, *et al.* conducted studies to determine the importance of bone mineral density in the performance of these systems [26]. Ladd, *et al.* conducted comparison studies on the pull-out strengths of lateral mass and pedicle screws in the human cervical spine. They reported that the cervical pedicle screws showed a significantly higher resistance to pull-out forces than the lateral mass screws [27].

In this study, an attempt was made to determine the moment of inertia and the angular acceleration of the entire spinal construct. This did not include the influence of the saw bone structure or factors such as bone density and rigidity of the spinal construct. The areas of the set screws once they have been torqued were calculated using digital image analysis. The shear stress, polar moment of inertia and eventually the torque was calculated using the distortion energy theory and fully plastic torque. The study also includes determining the torque

using a torque wrench. Suitable fixtures and adaptors were designed and developed for this purpose.

This part of the study also included conducting a test using multiple accelerometers on a multi-level construct to determine g-forces acting on the medium surrounding the pedicle screw head being torqued off.

2.1 G-Force Measurement Tests and Validation

The pedicle screw fixation system used for the accelerometer and high speed camera testing consists of pedicle screw, connectors, rod and set screw as shown in Figure 7. The process of breaking of the set screw is termed as the “event” and is usually performed by using manual torquing instruments as shown in the Figure 8.



Figure 7: Pedicle Screw Implant



Figure 8: Torquing Instruments

2.1.1 G-Force Accelerometer Test Set-up

A smaller spinal construct was set up on the optic table and instrumented using accelerometers and a 100 MHz digital oscilloscope as shown in Figure 9. Data was stored as a *.csv file and as a *.bmp file for a quick review.

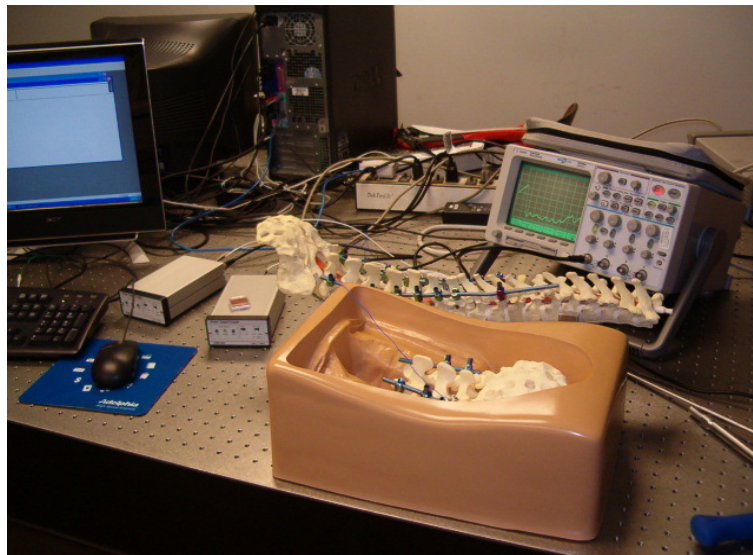


Figure 9: Laboratory Set-up

2.1.2 Fixtures

Two new fixtures were designed specifically to attach the accelerometers to the spinal construct. The first one (shown in Figure 10 and called Fixture 1) is used to attach the accelerometer to measure the tangential acceleration of the screw housing the set-screw that is being torqued off. On this screw the tangential acceleration is the larger component during the release of energy during the event, hence it provides sufficient information to get an estimate of the

g-forces. Further, it is extremely difficult to attach another accelerometer on the screw to measure the smaller radial component. The fixture fits on to the lower part of the pedicle screw head, and two set screws 180 degrees apart can be used to tighten the fixture on the screw head. It has been designed so it can slide in from any angle, and even if one set screw is accessible, it can be tightened to firmly fix the fixture to the screw head. The accelerometer can then slide in from either direction, such that it is perpendicular to the radial direction, and can then measure the tangential component of the acceleration. Wax was still used to firmly attach the accelerometer to the fixture, but it was constrained in the direction of motion by the fixture itself. The fixture weighs 7.9 grams and houses the accelerometer 15 mm away from the center of rotation.



Figure 10: Fixture 1 for Accelerometer

Shown below (in Figure 11) is Fixture 1 as it is installed below the set-screw. The accelerometer slides into the fixture and is pointed in the direction so as to measure the tangential acceleration component.

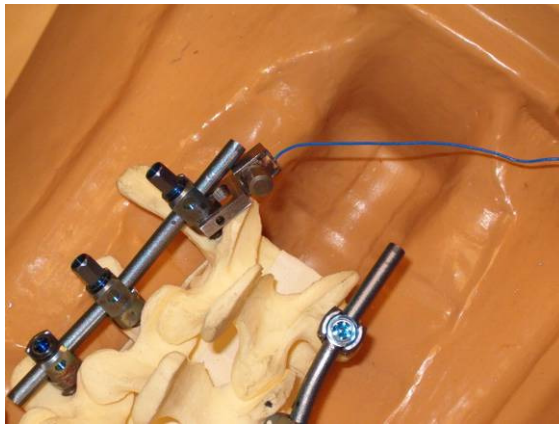


Figure 11: Installation of the fixture and accelerometer

The new fixture was used to collect numerous sets of data to see the reliability and the repeatability of the data. The two extreme set-screws (away from the base) were used as test specimens. The equipment used for the tests are (specifications for the equipments are given in Appendix B):

- An Agilent Digital Oscilloscope – 100 MHz with the ability to store data on a floppy disc as well as download it to a computer through a serial port at 9600 baud rate.
- Kistler accelerometers that have a resolution of 10 mV/g and a total weight of 3.2 grams. They have their own signal conditioning boxes such that the output is in Volts that can be then directly correlated to g-forces.

2.1.3 Bench Results for Accelerometer Tests

Figure 12 shows the results of the first test. As seen from the graph, the peak occurs at 5V which is about 500g of acceleration. The event duration was approximately 100 microseconds for the test.

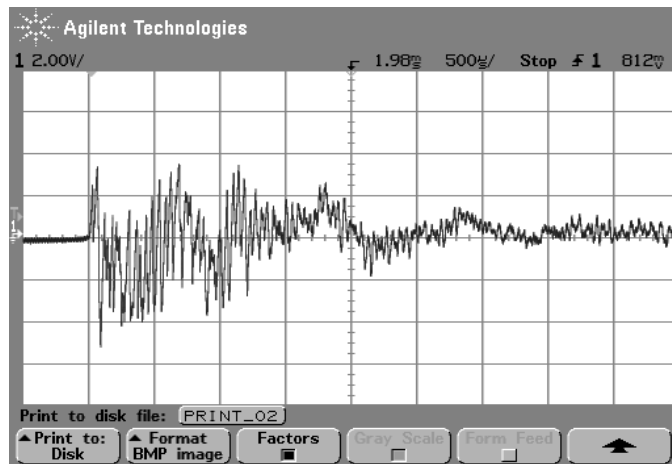


Figure 12: Results of Test 1 showing 500g acceleration

Figure 13 shows the results of the second test. The peak occurs at 6V which is about 600g of acceleration with the event duration being about 100 microseconds.

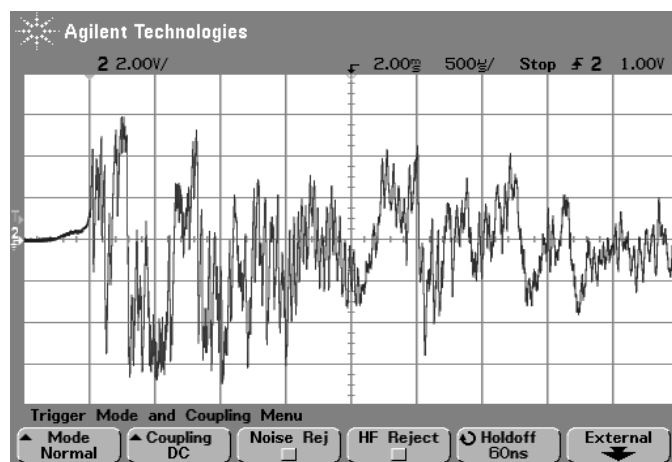


Figure 13: Results of Test 2 showing 600g acceleration

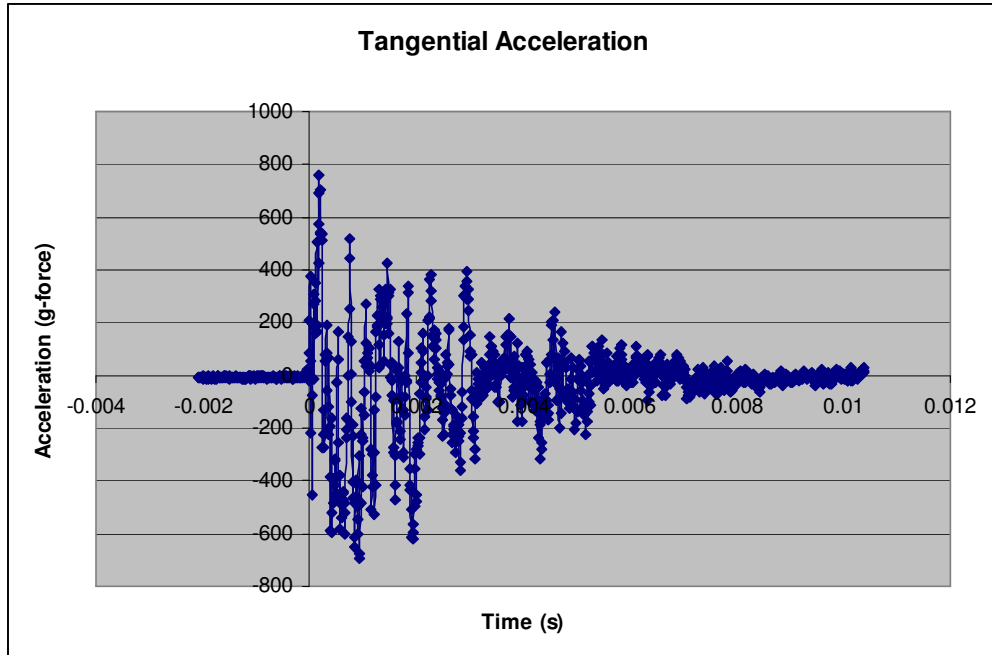


Figure 14: Test run that shows almost 800g acceleration

The results of the three tests illustrate the range of g-forces felt by the pedicle screw that houses the set-screw whose head is sheared off. In all the tests, the range of g-forces was found to be from 400g – 800g. The data shown in Figure 14 was collected while a high speed camera was used to capture the event.

2.1.4 Extended G-force Measurements Tests

The next series of tests were run to investigate the level of dissipation of the energy (g-forces from the point of release to different parts of the spine as well as the surrounding media). Hence four sites were selected as points for investigation:

1. The pedicle screw head itself, i.e. the one for which the set screw is being torqued off.
2. The center of the spine.
3. A pedicle (part of the spine) on the opposite side of the spine to one where the set screw is being torqued off.
4. The surrounding media, in this case the rubber holding case for the sawbone model.

2.1.5 Extended G-force Test Set-up

A test to determine G-forces on a multi-level construct was performed using accelerometers placed in different positions. The accelerometers are numbered as given below (A1-4) and are shown on a photograph in Figure 15. Kistler accelerometers and a 4-channel Agilent Oscilloscope were used in the experimental set-up as shown in Figure 16. The set screw (A1) was torqued off as shown in Figure 17 and the event data was captured using oscilloscopes.

A1 - Accelerometer 1: Screw head itself

A2 - Accelerometer 2: Center of the spine

A3 - Accelerometer 3: Pedicle on the opposite side of the spine

A4 - Accelerometer 4: Surrounding media

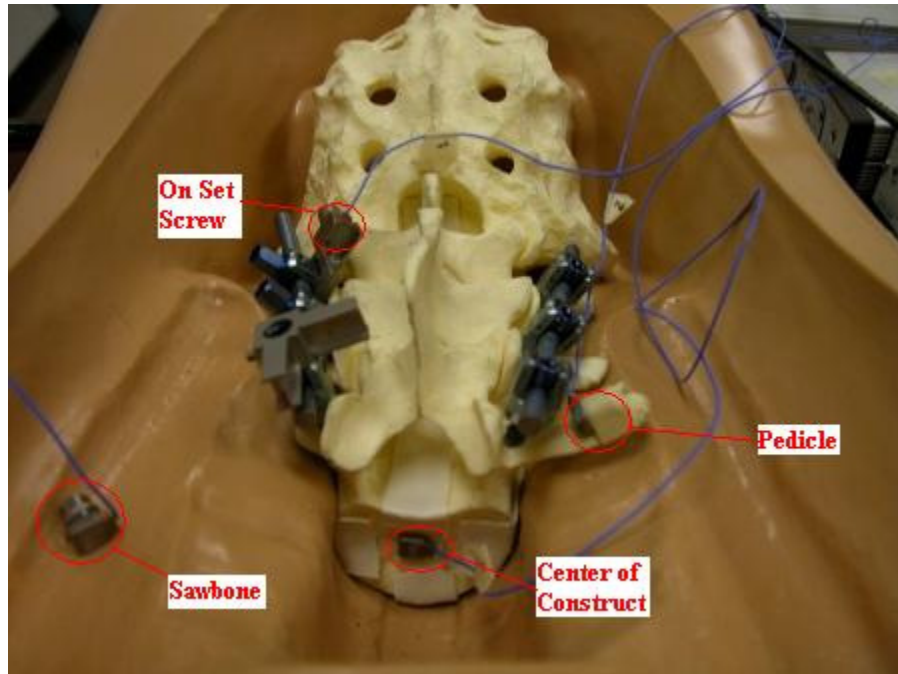


Figure 15: Accelerometer placed on smaller multi-level construct



Figure 16: Set-up for multi-level construct test

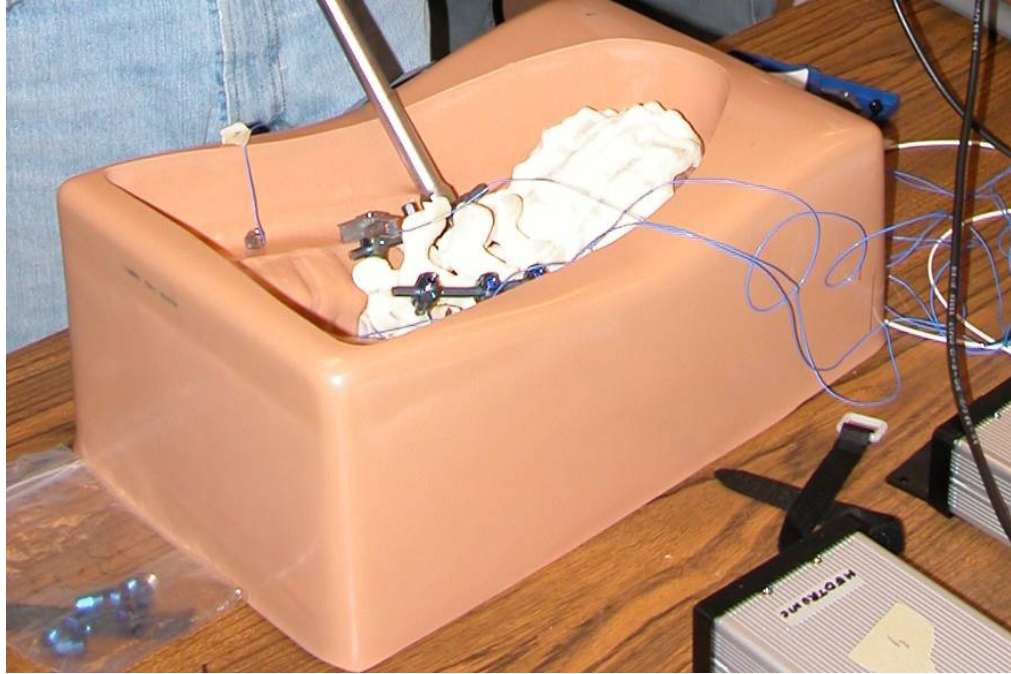


Figure 17: Torquing of the set screw

2.1.6 Test Results

Three tests were performed using the test set-up and the event duration for each was approximately 100 milliseconds. Maximum g-force values were obtained for the four accelerometers placed in their respective positions from each of the tests. An average of the g-forces was calculated and the results were plotted. Table 1 shows the experimental data obtained for each of the tests and their average. As can be seen in Figure 18, the maximum g-forces are felt on the screw on which the set-screw is being torqued off (150-250 g's). The center of the spine barely experiences 10-50 g's, and a pedicle on the other side of the spine experiences 10-16 g's. The surrounding medium, in this case, the rubber housing, experiences negligible accelerations in all three tests (less than 1g).

Table 1: Multi-level Construct Test Data

	Test 1	Test 2	Test 3	
Accelerometer Readings	Maximum G-force	Maximum G-force	Maximum G-force	Average G-force
Accelerometer 1 (On Screw)	150.04	241.94	177.63	189.87
Accelerometer 2 (Center)	6.08	17.10	44.66	22.61
Accelerometer 3 (On Pedicle)	10.99	9.78	15.90	12.22
Accelerometer 4 (On Sawbone)	0.92	0.92	0.92	0.92



Figure 18: Maximum g-forces at different locations

Figure 19, which is the plot for the average of the three tests, clearly shows how quickly the g-forces die down as one moves away from the set-screw that is being torqued off.

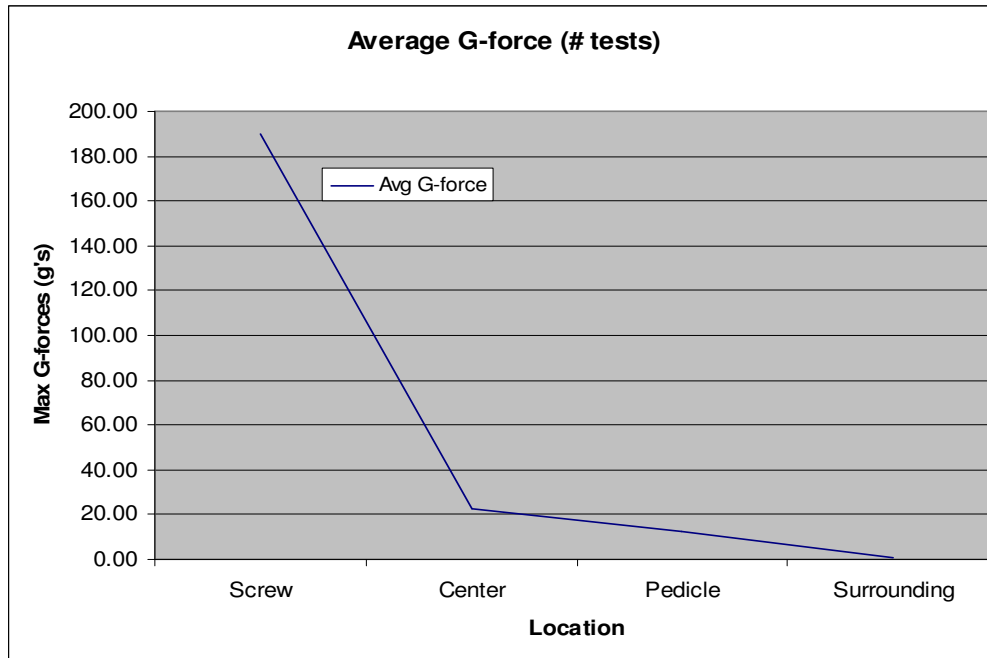


Figure 19: Average of the maximum g-forces

2.1.7 High Speed Camera Test Set-up and Results

Three high speed cameras, one each from Vision Research [28], Motion Engineering [29] and Olympus i-speed [30] as shown in figures 20, 21 and 22 respectively were used to capture the event.

Cameras used to capture the event



Figure 20: Vision Research



Figure 21: Motion Engineering



Figure 22: Olympus i-speed 3

The specifications for these cameras are given in Appendix B. The test set-up using each of these cameras is shown in figures 23, 24 and 25 below:



**Figure 23: Vision Research Camera
Test Set-up**



**Figure 24: Motion Engineering Camera
Test Set-up**



Figure 25: Olympus i-speed 3 Camera Test Set-up

2.1.8 Validation Using High Speed Camera

Numerous tests were conducted, but for conciseness, only one test from the Olympus i-speed 3 camera is discussed here. The camera resolution used was 264 by 196 pixels with 40000 frames-per-second. The exposure time for the test was $6\mu\text{s}$. The accompanying Track Eye Motion Analysis (TEMA) software was used for image analysis as shown in Figure 26 [31].

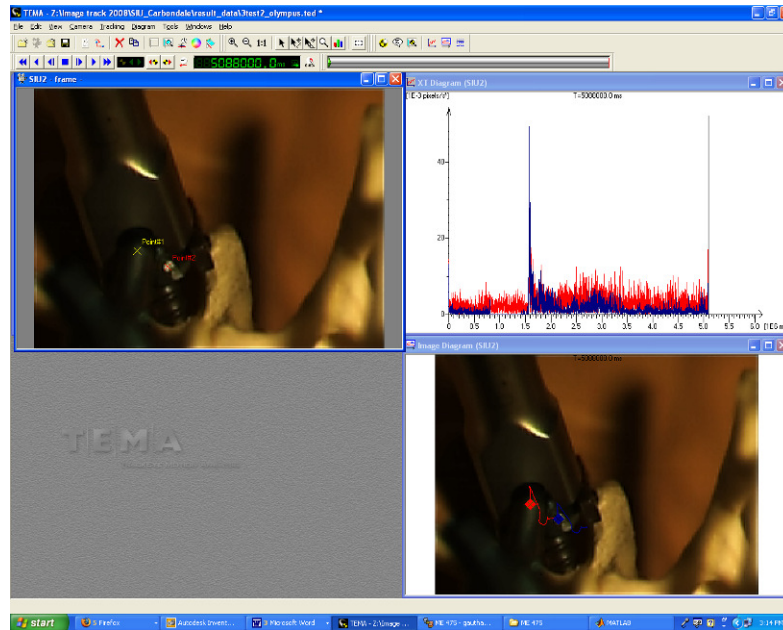


Figure 26: Track Eye Motion Analysis (TEMA) software [31]

Two points were marked on the construct, their positions are shown by the two arrows as shown in Figure 27. The TEMA software was then used to extract the displacement, velocity, acceleration of the two points as well as the path of the points as shown in Figure 28.

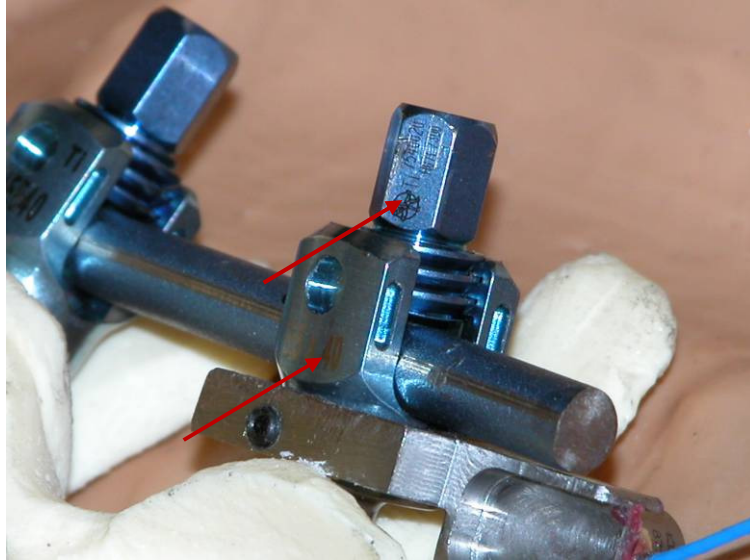


Figure 27: Two points marked on the construct

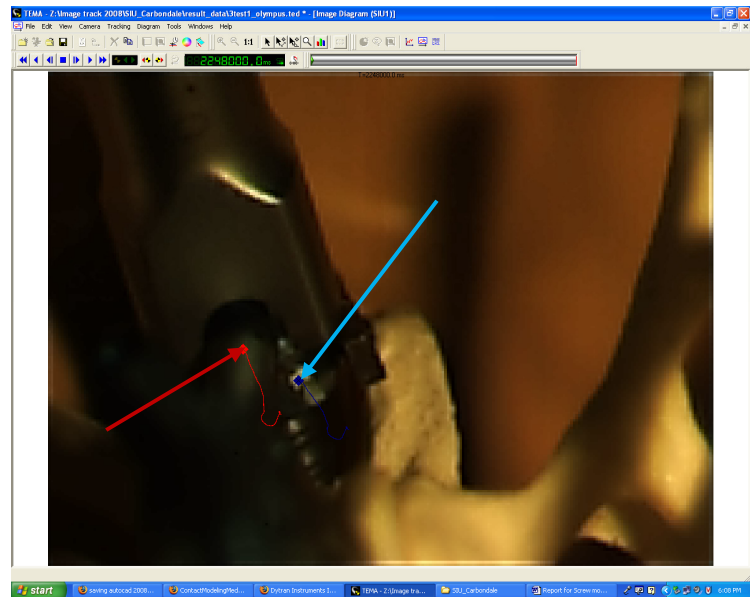


Figure 28: Path of the two points marked in red and blue

The TEMA software is capable of providing the X and Y displacement, velocity and acceleration plots. It can also provide an absolute plot, but those are not presented. It is the acceleration plot that is of interest, and needs to be correlated with the accelerometer output during the test. A total of 5089 frames were captured from the Olympus i-speed 3 test and analyzed using the TEMA software. The resulting plots of the X and Y direction displacement, velocity and acceleration are shown in figures 29 – 34. The 'x' axis is in milliseconds and the 'y' axis in pixel measurement. Figure 35 shows the X direction acceleration from the accelerometer test which is correlated with the X direction accelerometer plot obtained from TEMA.



Figure 29: X direction Displacement from TEMA

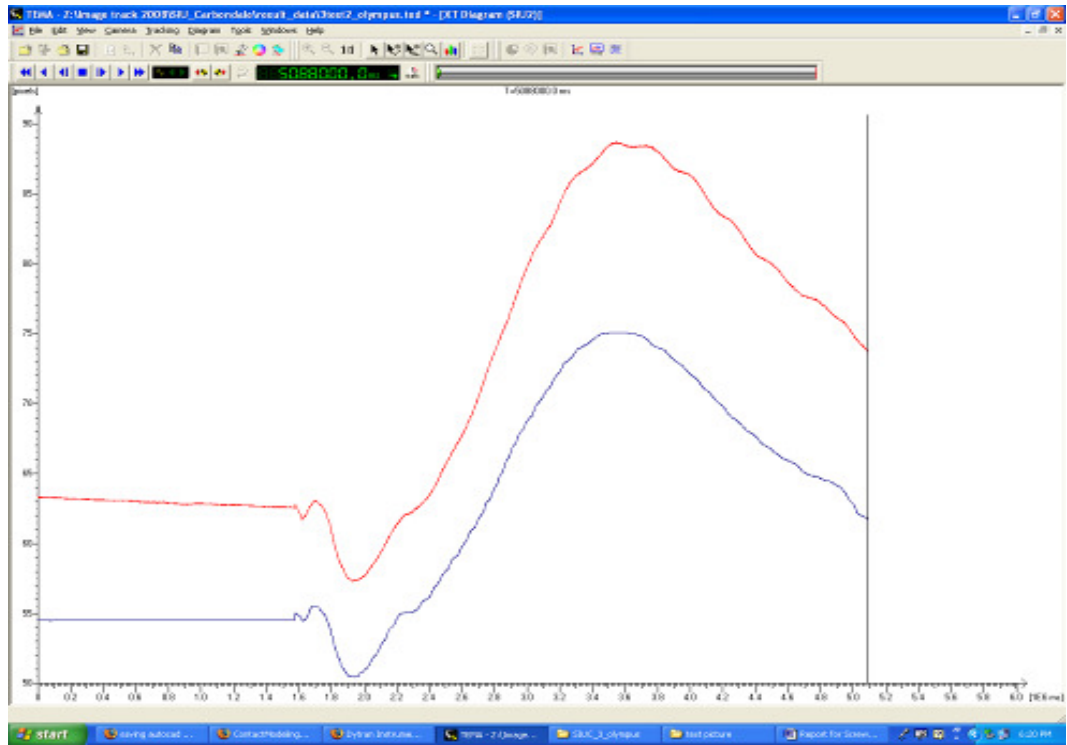


Figure 30: Y Direction displacement from TEMA

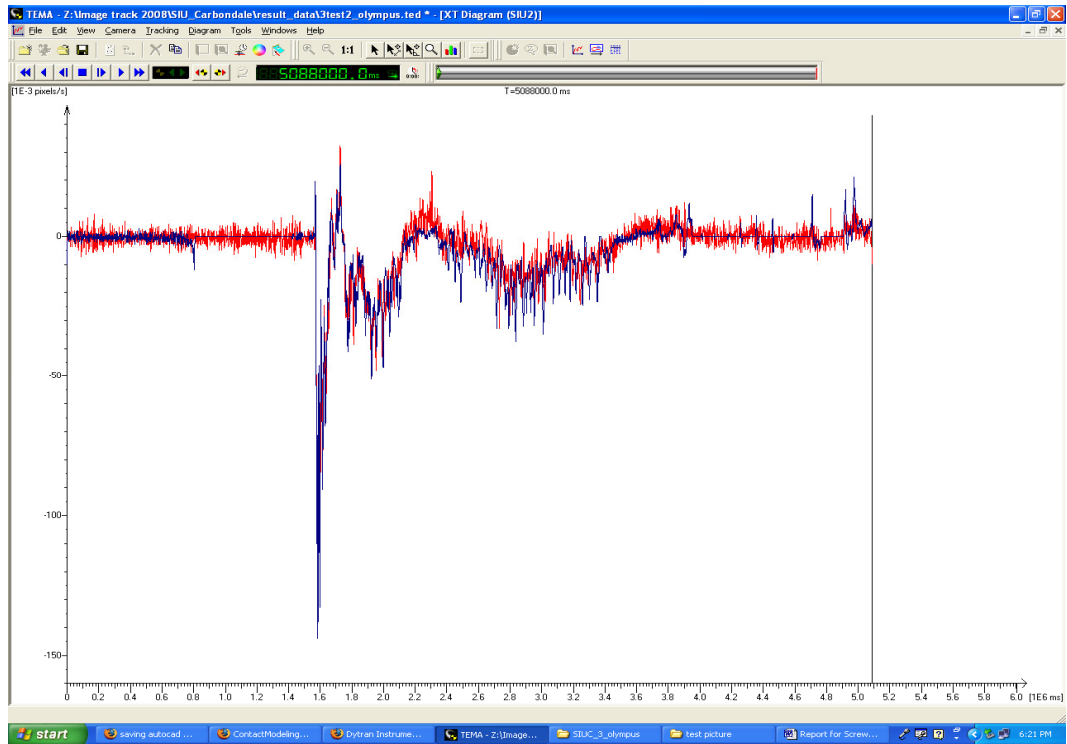


Figure 31: X Direction Velocity from TEMA

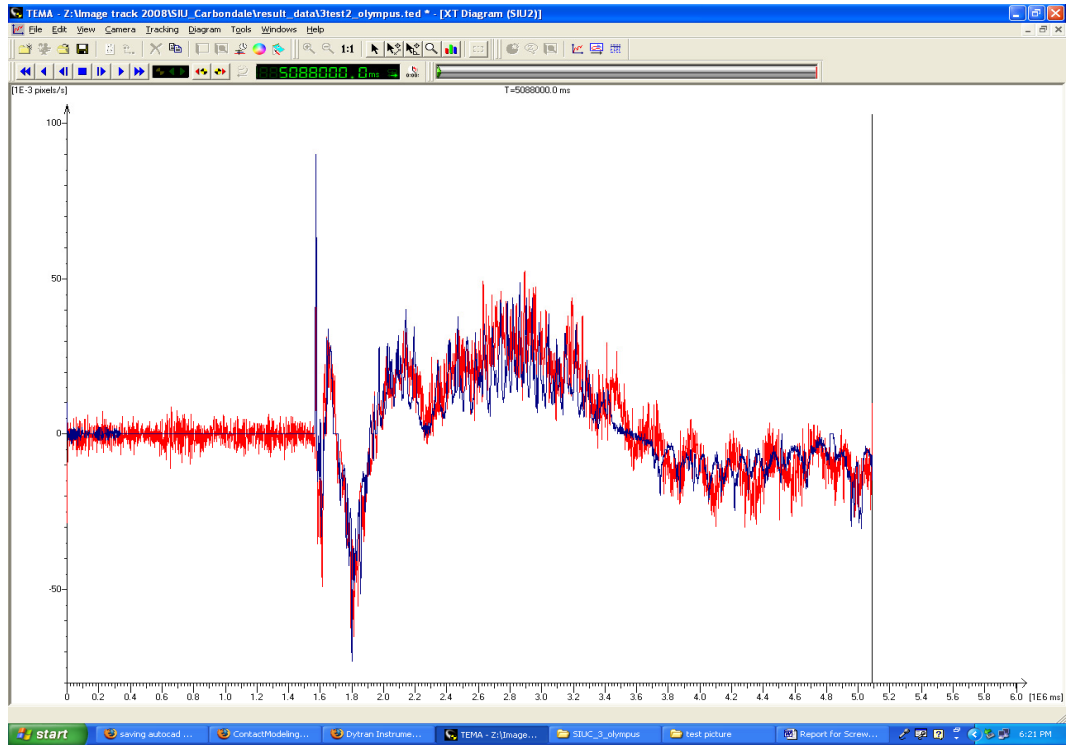


Figure 32: Y Direction Velocity from TEMA

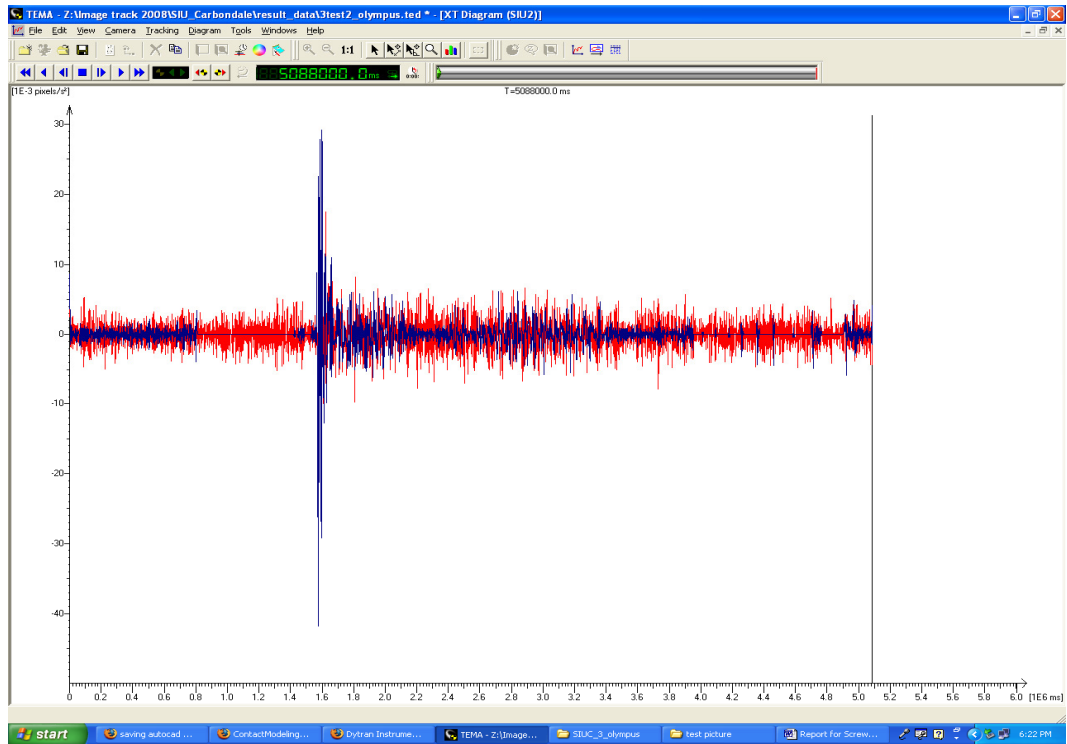


Figure 33: X Direction Acceleration from TEMA

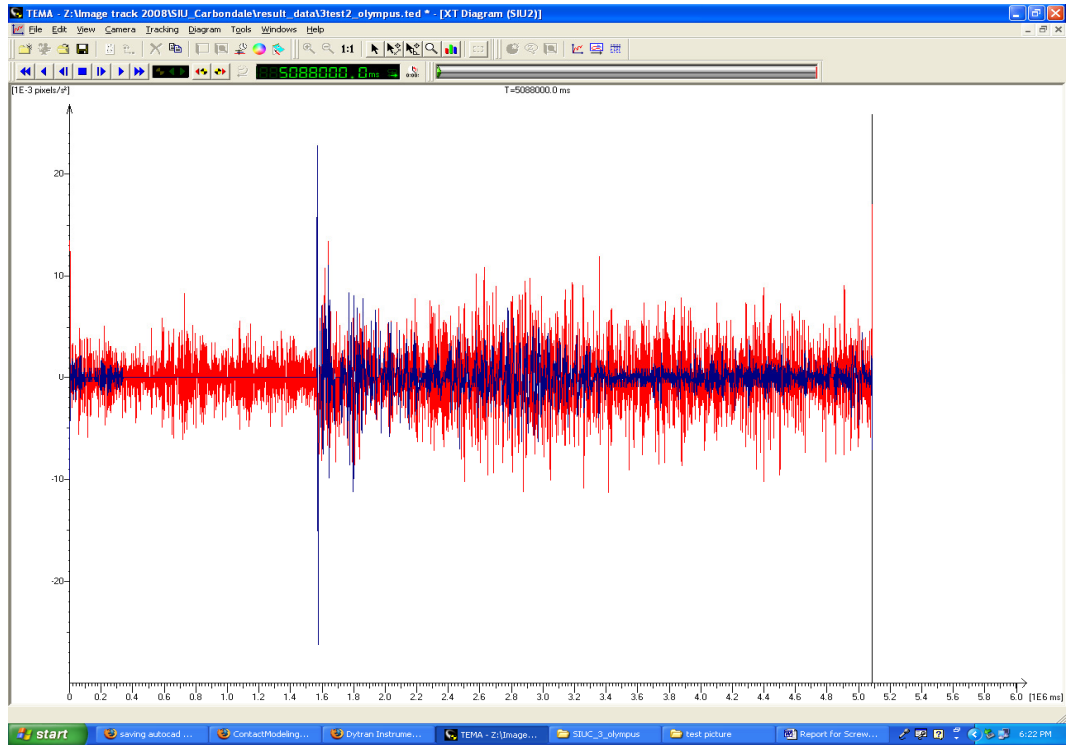


Figure 34: Y Direction Acceleration from TEMA

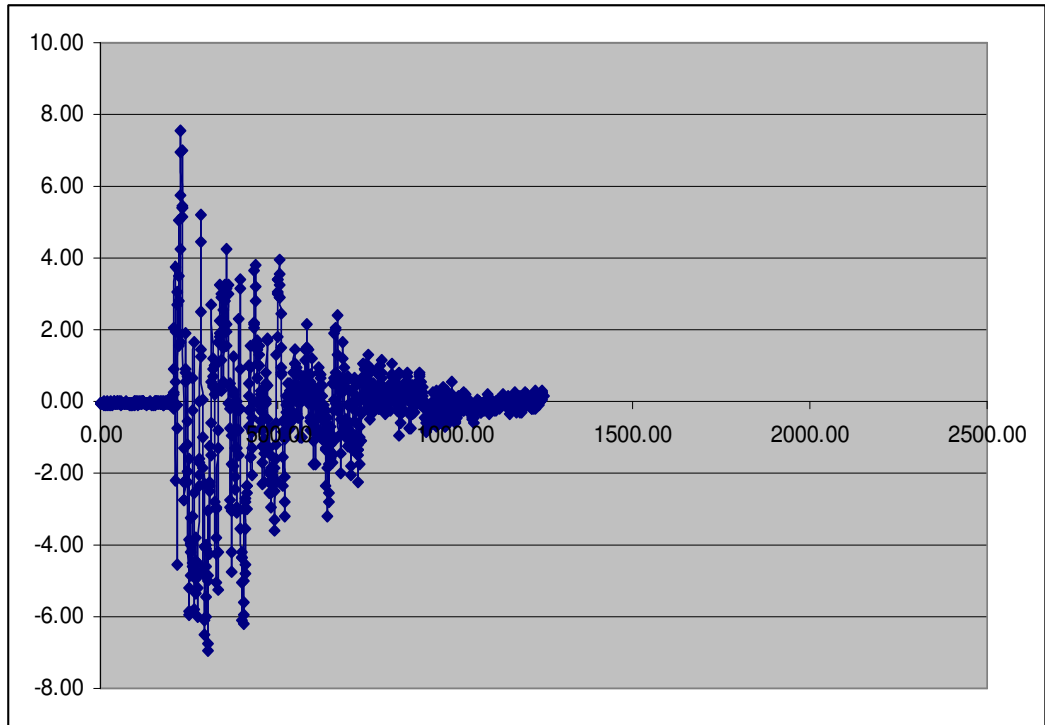


Figure 35: X direction acceleration (accelerometer)

2.2 Measurement of Torque and Results

The break-off torque was estimated using the distortion energy failure theory (DET) for ductile materials, fully plastic torque (FTP) and was further measured using a torque wrench. Both of these numbers were then compared to the design value supplied by Medtronic to validate the work done in this project.

2.2.1 Distortion Energy Theory (DET)

Distortion Energy Theory states that “yielding occurs when the distortion component of the strain energy per unit volume reaches or exceeds the distortion strain energy per unit volume at the yield point in a simple tensile or compression test” [32].

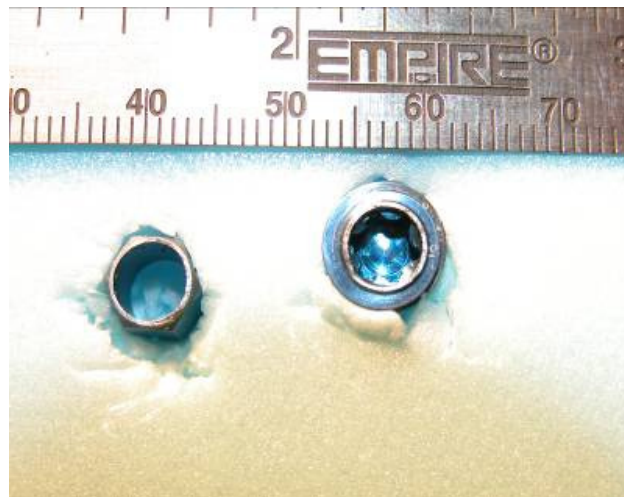


Figure 36: Set Screw heads in foam with measurement scale

Digital image analysis was used to estimate the inner and outer diameters of the fractured areas. Two set screws were fixed within foam and a digital image was taken, and then analyzed using customized software. In figure 36 above, the screw head on the left is attached to the set-screw on the right. The image of screw on the left is after it has been torqued off from the top of the screw on the right. Using digital image analysis, inner and outer diameters were measured and were validated using a Digital Micrometer. The inner diameter (D_i) was calculated to be 0.005235m whereas from the micrometer measurement, it was found to be 0.0053m. The outer diameter (D_o) was calculated to be 0.0061111m whereas from the micrometer measurement, it was found to be 0.0061m. Table 2 shows the inner and outer diameter values obtained from digital image analysis and their validation using a digital micrometer.

Table 2: Inner and Outer Diameter values

Parameters Measured	From Digital Image Analysis	Validation from a micrometer
Inner diameter (d_i)	0.005235 m	0.0053 m
Outer diameter (d_o)	0.0061111 m	0.0061 m

Figure 37 depicts the inner and outer diameter in a hollow cylinder and also shows the stress distribution.

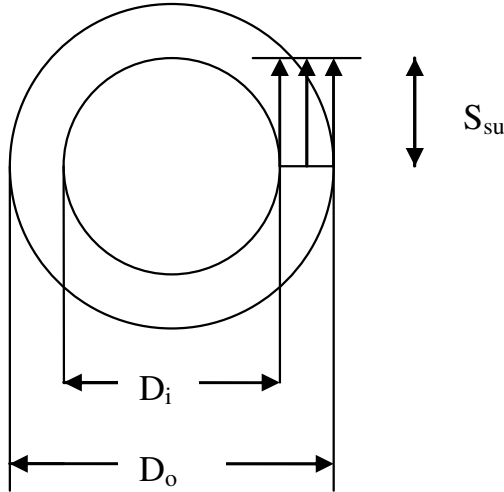


Figure 37: Inner, Outer Diameter and Stress Distribution in a cylinder

The area of the hollow circle was found to be $7.16283E-06 \text{ m}^2$. The value of Ultimate Tensile Strength S_{ut} for Titanium alloy Ti-6Al-4V is 1040 MPa [33]. From the Distortion Energy Theory, we have the equation for tensile strength as:

$$S_{su} = 0.57735 S_{ut} \quad (3.2)$$

The tensile strength was calculated to be 600.444 MPa

The force is given by the equation 3.3 [32]:

$$F = S_{su} A \quad (3.3)$$

The force was calculated to be 4300.88 N. The break-off torque for hollow torsion members (D_m as the mean diameter) is given by the formula [32]:

$$T_{break-off} = F * D_m / 4 \quad (3.4)$$

The value of the break-off torque was 12.26 N-m.

2.2.2 Fully Plastic Torque (FPT)

For fully plastic materials, Torque is calculated by equation 3.5 [34]:

$$T_{FP} = T_{PS} - T_{PH} \quad (3.5)$$

Where,

T_{FP} = fully plastic torque of a solid torsion member.

T_{PS} = fully plastic torque of a solid torsion member having the outer boundary condition.

T_{PH} = fully plastic torque of a solid torsion member having the inner boundary condition.

T_{PS} is calculated by the formula [34]:

$$T_{PS} = 2\pi S_{su} (D_o/2)^3 \quad (3.6)$$

The value of T_{PS} was calculated to be 35.68 N-m.

T_{PH} is calculated by the formula [34]:

$$T_{PH} = 2\pi S_{su} (D_i/2)^3 \quad (3.7)$$

The value of T_{PH} using the above equation was 23.40 N-m. **The break-off torque T_{FP} for fully plastic materials was found to be 12.28 N-m.**

2.2.3 Torque Measurement Using a Torque Wrench

A torque wrench from Craftsman as shown in Figure 38 was also used to measure the break-off torque [35].



Figure 38: Torque Wrench from Craftsman® [35]

The break-off torque from this instrument was 11.3 N-m.

2.3 Results – Comparison of G-Force and Torque

The following table 3 shows the comparison of G-force values obtained from accelerometer measurements and high-speed cameras. The g-force value from the high speed camera test was calculated based on the resolution of the camera. The results show that the high speed camera provides data for the accelerations that are very comparable to those provided by the accelerometers.

Table 3: Comparison of G-Force Values

Method No	Method	G-force Value m/s ² (g)
1	Accelerometer Test	7848 (800g)
2	High Speed Camera Test	8160 m/s ² (832g)

The following table 4 shows the comparison of break-off torque values obtained from Distortion Energy Theory for ductile materials and by using a torque wrench in comparison with the actual design break-off torque value supplied by Medtronic.

Table 4: Comparison of Torque Values

Method No	Method	Torque Value (N-m)
	Design break-off torque (as supplied by Medtronic)	11.00 N-m
1	Distortion Energy Theory (DET)	12.26 N-m
2	Fully Plastic Torque (FTP)	12.28 N-m
3	Torque Wrench	11.30 N-m

2.4 Summary on G-Force and Torque Measurements

This section provided results for the acceleration measurements in a spinal construct during the event of the breaking of the set-screw head. The data was collected by using specially designed fixtures that are fixed on to the pedicle screws and allows for the easy installation of accelerometers. Two types of fixtures were designed, one for the set screw that is being torqued off, while another that can be mounted on adjoining set screws/pedicle screws. Data was only collected from the screw whose set-screw was being torqued off. The data recorded showed high g-forces, in the range of 400-800g's using the manual torquing instrument. These measurements were validated using a high speed camera that also showed the movement of the different points-of-interest on the construct. The section further provides a complete solution in the understanding of the event by correlating the design torque (11 N-m) required for breaking the set-screw to the torque calculated from the distortion energy theory for material fracture (9.9 N-m) and an actual measurement using a torque wrench (11.3 N-m). The study conducted to determine the maximum g-forces in subsequent screws in a multi-level construct indicated that screws adjacent to the set-screw being torqued off were also subjected to deteriorating g-forces. This study provides an in-depth analysis of the event which can be used for improved design of the spinal constructs and instrumentation. The continuation of this project is reported in the chapter 4 that outlines how the work done in this section was used to compare the performance of the manual instrument to a powered one, where the data was collected from tru-trainers and cadavers.

CHAPTER 3 – NEUROSURGICAL POWERED AND MANUAL TORQUING INSTRUMENT PERFORMANCE COMPARISON

This section discusses performance comparisons between a manual torquing instrument and a powered prototype used in spinal constructs in neurosurgery.

A study was conducted as part of this research to determine the bench results on the G-force measurements during manual torquing of the set screws. This study as described in Chapter 2 reported the g-forces and torques acting on the pedicle screw system theoretically as well as experimentally [36].

In the recent past, human cadaveric spinal models have been used successfully for several studies regarding pedicle screw fixation systems. Wiesner, et al. [37] conducted in vitro experiments using human cadaver models to determine the accuracy of two different techniques of percutaneous pedicle screw insertion in the lumbar spine. Their study showed that the percutaneous pedicle screw insertion technique in the lumbar spine was a safe and reliable method. Elliot et al. [38] performed a laboratory study to analyze the pedicle screw placement using a freehand technique without image guidance in cadaveric specimens. Their study showed that the results of the technique were equal or better than those cadaver studies that used guidance systems. A manual tool invented by Roger P. Jackson for use in installing osteosynthesis devices consists of socket type tools with a handle, stem and a socket head [39]. A tool for insertion, adjustment and engaging implants such as a polyaxial screw

implant was devised by inventors Nam T. Chao, Chris Rybicki and Dale Whipple [40]. Various manual tools for placement of pedicle screws and removal of the set screw heads have been developed by different companies specific to their pedicle screw fixation system devices.

In this study, an attempt was made to determine the G-forces acting on the implant placed in human cadaver spines and also on tru-trainers. Two separate stations, 3Dx and G4 were used for this purpose. Each station had one cadaver and one tru-trainer. Suitable fixtures and adaptors designed and developed to house the accelerometers were used to capture the data.

The main performance criterion used is the g-forces felt on the pedicle screw that houses the set-screw which is being torqued off, as well as adjoining screws on the construct. The process, termed as the event, is primarily a release of energy as the head of the set screw breaks off. Data collected from bench tests shows high g-forces, in the range of 400-800g, and these are verified by tru-trainer and cadaver experiments. Data collected from bench tests shows high g-forces, in the range of 400-800g, and these are verified by tru-trainer and cadaver experiments. The use of a new powered prototype is introduced in this study, and it is shown in this section that the powered instrument has the following advantages:

- a) Usually lower accelerations on the construct
- b) Faster die down time
- c) Reduced work done
- d) Higher consistency.

3.1 Tru-Trainer and Cadaver Laboratory Test Set-up

Two Stations 3DX and G4 were used in this study. Each of these stations had one tru-trainer and one cadaver each set up as shown in Figures 40 and 41. 5 surgeons named as Surgeon 1, Surgeon 2, Surgeon 3, Surgeon 4 and Surgeon 5 rotated through these two stations and provided 4 sets of data for each of the tru-trainer and cadaver studies using both manual and powered instruments. In total 40 data sets were obtained from the surgeons – 20 for the tru-trainers and 20 for the cadavers. Figure 39 shows the manual torquing instruments that consist of a break off driver that retains the set screws and a counter torque.



Figure 39: Manual Torquing Instruments



Figure 40: Tru – Trainer Laboratory Set-up

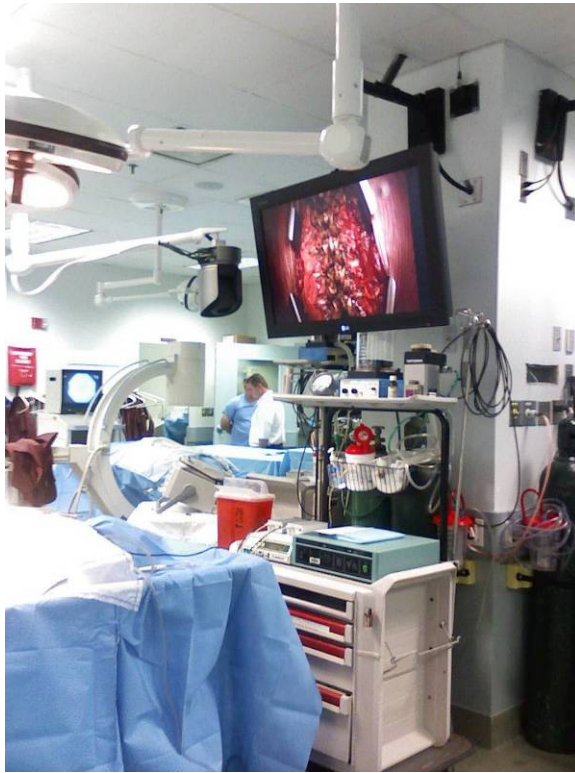


Figure 41: Cadaver Laboratory Set-up

3.2 Tru-Trainer and Cadaver Lab Data Analysis

Two accelerometers attached at right angles on the adjoining screw to provide x and y direction G-force measurements were used to collect the data. These were then converted to single vector estimation (rms value). The data was then analyzed to provide comparisons between the manual and the powered instrument based on the following four performance criteria:

- a. Maximum g-force felt on the adjoining screw during torquing off.
- b. Time taken for the g-forces to die down (95% reduction time).
- c. Total energy felt at the adjoining screw (or work done) – this was obtained by integrating the curve for the g-forces.
- d. Consistency – obtained by comparing the standard deviation in the work done.

3.2.1 3Dx Station (Manual/Powered Instrument Test Analysis)

This section describes the details of analysis for a single data set from a cadaver experiment performed by Surgeon 1 on the 3Dx station using both manual instruments and the powered prototype.

The data obtained in the form *.csv files were exported onto Microsoft Excel program for analysis. The data included the time and the two accelerometer readings. Figure 42 shows the plots of the two accelerometer

readings (x and y directions) against time obtained from the manual instrument test and figure 43 shows the trend lines associated with the plots. A moving average of 10 was used to smooth the fluctuations in data, thus showing the trend more clearly. The root mean square (rms) value of the two voltages was calculated to get a vectorial representation of the g-forces in the plane of the motion. The resulting data points were plotted against time as shown in Figure 44. The figure also shows the location of the rms value of the maximum g-force and the die-down time (at 95% reduction of the g-forces). A moving average of 10 used to more accurately predict the trends in the rms data. Figure 45 shows the graph which depicts the approximate area under the curve to calculate the work done.

A similar analysis was conducted for the 3Dx Cadaver data set using a powered prototype. Figure 46 show the plot of accelerometer readings against time while figure 47 depicts the trendline plot associated with the accelerometer readings. Figure 48 shows the rms against time plot and figure 49 describes the area under the curve.

A sample set of data has been provided in Appendix A. The raw data for all the surgeons are provided in Appendices C, D, E, F and G.

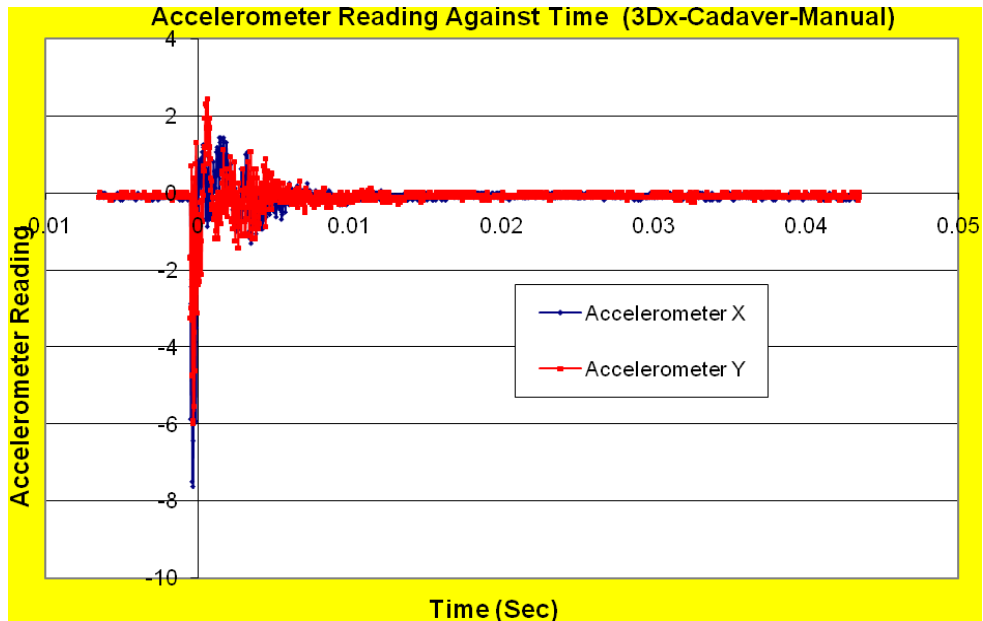


Figure 42: Plots of Accelerometer readings against time

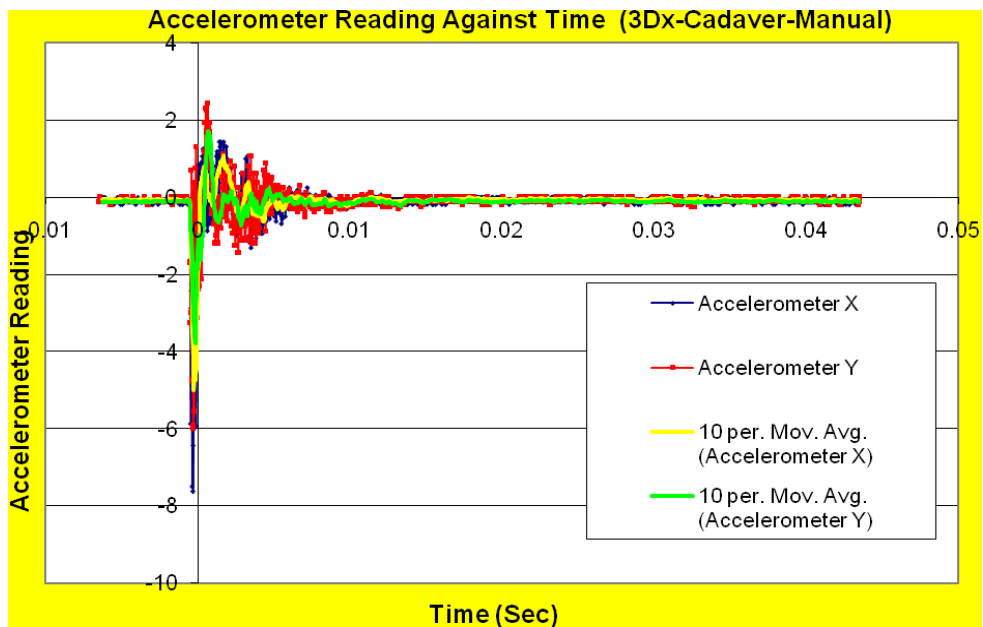


Figure 43: Trendlines of the accelerometer readings against time

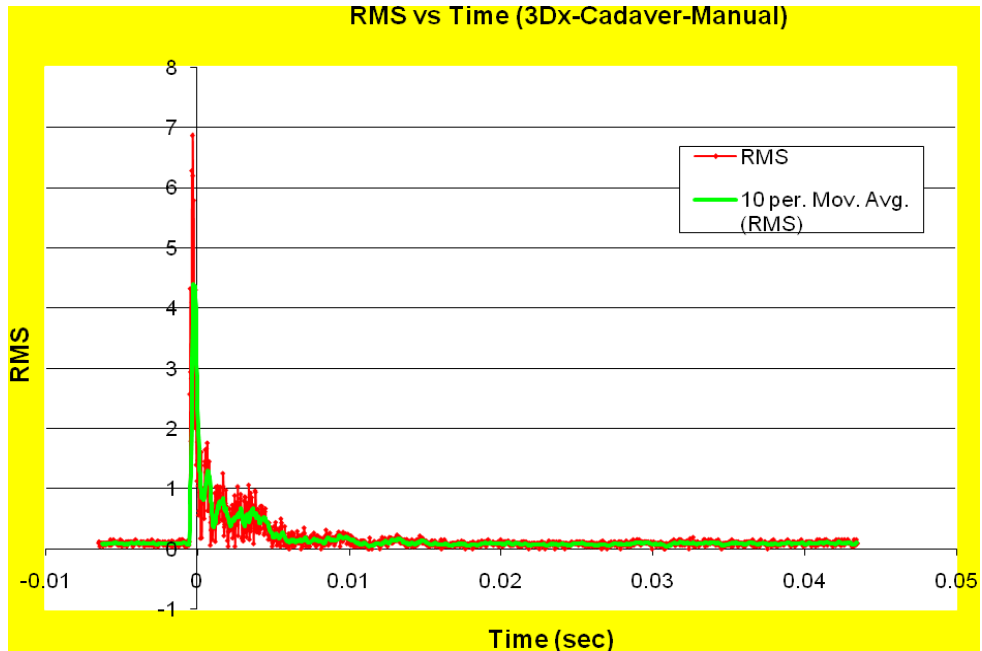


Figure 44: Plot of RMS value and Trend line

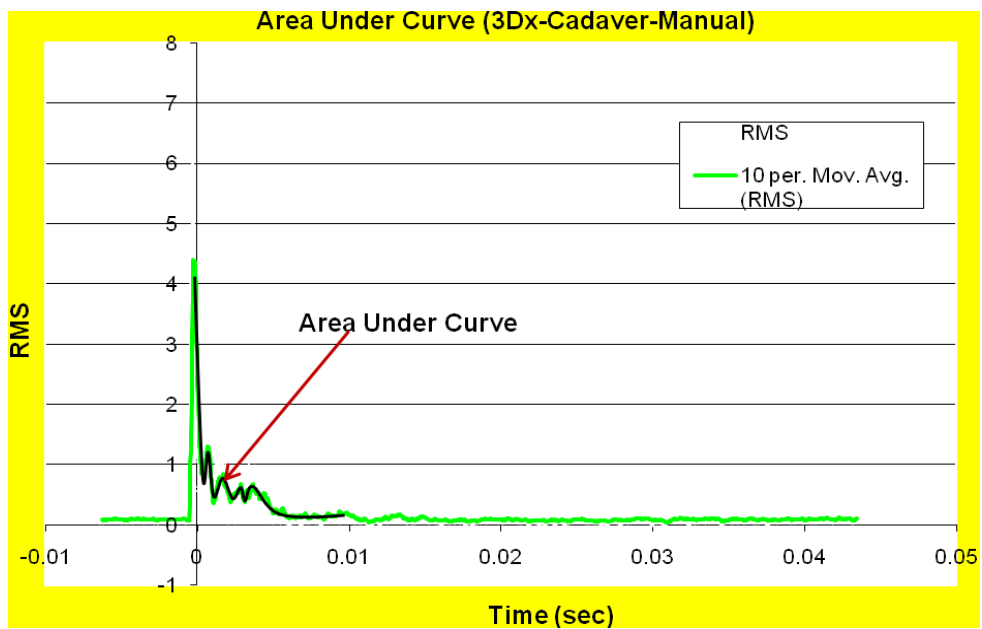


Figure 45: Spline used to identify area under curve

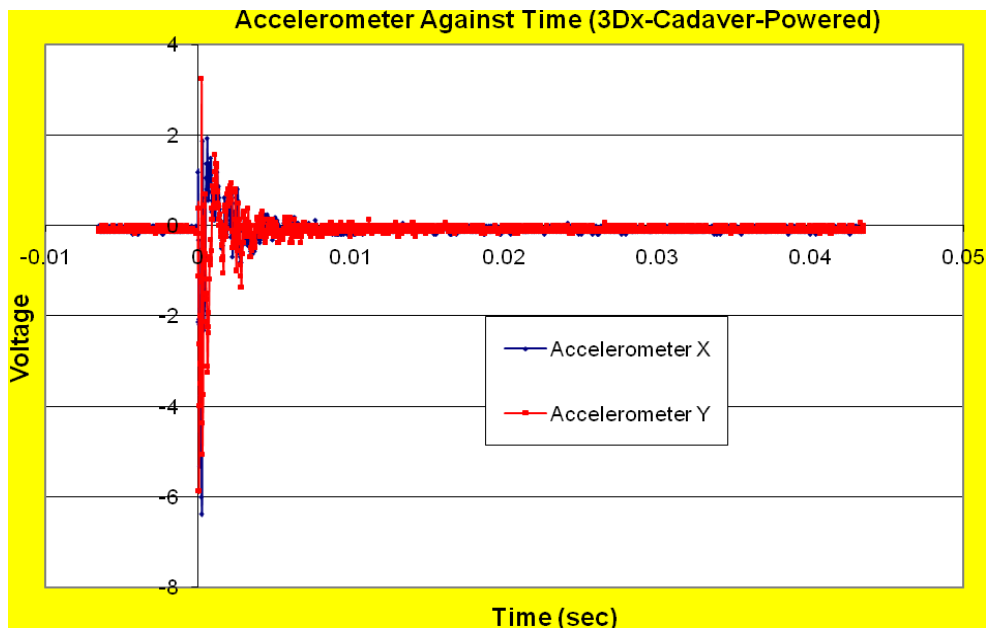


Figure 46: Plots of Accelerometer readings against time

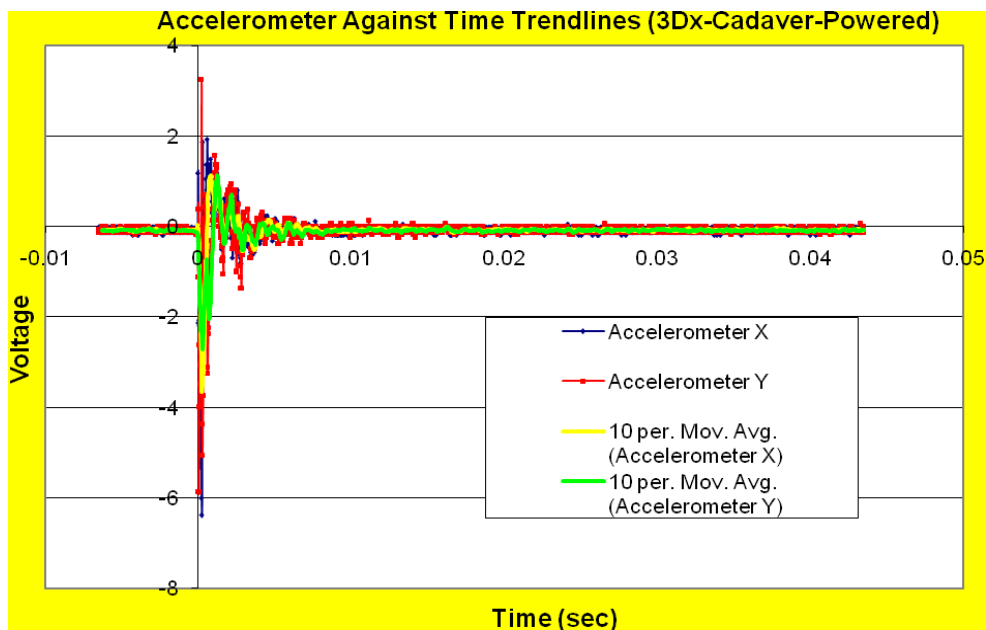


Figure 47: Trendlines of the accelerometer readings against time

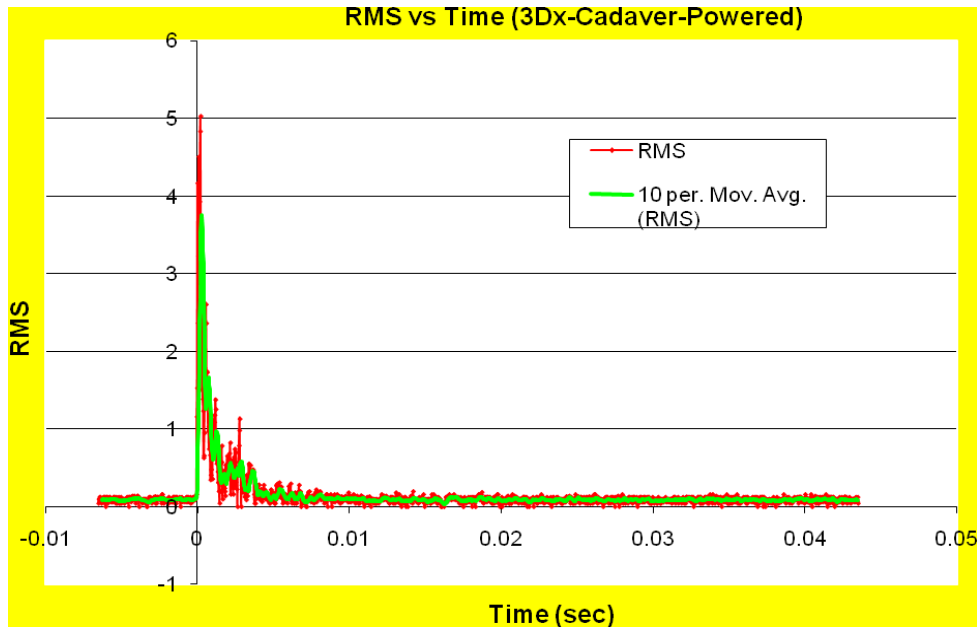


Figure 48: Plot of RMS value and Trend line

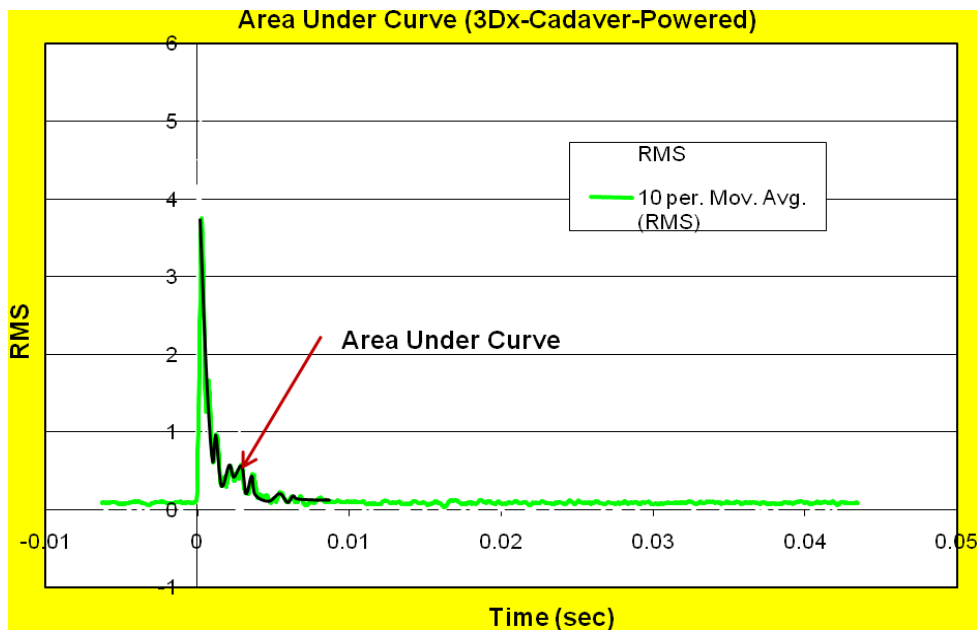


Figure 49: Spline used to identify area under curve

3.2.2 Data obtained from Surgeons

Table 5 and Table 6 shows the cadaver and tru-trainer performance data obtained from Surgeon 1 using the manual and powered instruments on both 3Dx and G4 stations. Similarly Table 7 and Table 8 shows the performance data obtained for Surgeon 2, Table 9 and Table 10 for Surgeon 3, Table 11 and Table 12 for Surgeon 4 and Table 13 and Table 14 for Surgeon 5.

These tables provide the values of the maximum g-forces, the 95% die-down reduction time and the work done. The values were obtained by using the rms-time plot. The maximum rms value was considered as the maximum g-force value. The 95% die-down reduction time was calculated as the time for the maximum g-force value to reduce to 95% of its original value. The area under the curve was calculated and this was taken to be the work done. Composite Trapezoidal rule was used to approximate the area under the curve. A MatLab code H was used to obtain the area under the curve.

Table 5: Performance Data by Surgeon 1 using a Tru-trainer

Performance Criteria	TRU-TRAINER			
	Manual Instrument		Powered Prototype	
	3DX	G4	3DX	G4
Max G-Force	486	650.1	514.3	637.1
Die down	0.00372	0.008325	0.012225	0.00535
Work Done	0.0053	0.0178	0.0102	0.0105

Table 6: Performance Data by Surgeon 1 using a Cadaver

Performance Criteria	CADAVER			
	Manual Instrument		Powered Prototype	
	3DX	G4	3DX	G4
Max G-Force	686	254	501.9	106.7
Die down	0.0052	0.007395	0.005525	0.000995
Work Done	0.0094	0.002	0.0075	0.0028

Table 7: Performance Data by Surgeon 2 using a Tru-trainer

Performance Criteria	TRU-TRAINER			
	Manual Instrument		Powered Prototype	
	3DX	G4	3DX	G4
Max G-Force	445.7	512.1	534.2	484.4
Die down	0.0114	0.01595	0.00725	0.0107
Work Done	0.0106	0.013	0.0103	0.0103

Table 8: Performance Data by Surgeon 2 using a Cadaver

Performance Criteria	CADAVER			
	Manual Instrument		Powered Prototype	
	3DX	G4	3DX	G4
Max G-Force	616.7	665.5	440.2	447.4
Die down	0.00481	0.0032	0.00303	0.002995
Work Done	0.0051	0.0045	0.0034	0.0037

Table 9: Performance Data by Surgeon 3 using a Tru-trainer

Performance Criteria	TRU-TRAINER			
	Manual Instrument		Powered Prototype	
	3DX	G4	3DX	G4
Max G-Force	430	646	469	636
Die down	0.0177	0.01	0.00815	0.007075
Work Done	0.0112	0.0122	0.0095	0.0115

Table 10: Performance Data by Surgeon 3 using a Cadaver

Performance Criteria	CADAVER			
	Manual Instrument		Powered Prototype	
	3DX	G4	3DX	G4
Max G-Force	583	549	345	115
Die down	0.007475	0.00552	0.00775	0.000385
Work Done	0.0081	0.0065	0.0074	0.0033

Table 11: Performance Data by Surgeon 4 using a Tru-trainer

Performance Criteria	TRU-TRAINER			
	Manual Instrument		Powered Prototype	
	3DX	G4	3DX	G4
Max G-Force	538.4	574.7	592	581.6
Die down	0.0086	0.009375	0.005825	0.003775
Work Done	0.0129	0.0146	0.0111	0.0114

Table 12: Performance Data by Surgeon 4 using a Cadaver

Performance Criteria	CADAVER			
	Manual Instrument		Powered Prototype	
	3DX	G4	3DX	G4
Max G-Force	332.1	362.5	402.4	561.8
Die down	0.002188	0.00185	0.000585	0.00449
Work Done	0.0054	0.0032	0.003	0.0079

Table 13: Performance Data by Surgeon 5 using a Tru-trainer

Performance Criteria	TRU-TRAINER			
	Manual Instrument		Powered Prototype	
	3DX	G4	3DX	G4
Max G-Force	562.5	572	593.7	563.2
Die down	0.0059	0.00655	0.00585	0.006275
Work Done	0.0099	0.0143	0.0103	0.0114

Table 14: Performance Data by Surgeon 5 using a Cadaver

Performance Criteria	CADAVER			
	Manual Instrument		Powered Prototype	
	3DX	G4	3DX	G4
Max G-Force	609.4	670.1	336.1	596.8
Die down	0.006275	0.00126	0.00168	0.001288
Work Done	0.0045	0.0043	0.0031	0.0042

3.3 Data Comparison for Manual and Powered Prototype

Considering the data of Surgeon 1 as an example, the average of the rms values of the maximum g-forces was calculated for the cadaver and tru-trainer experiments on both 3Dx and G4 stations using the manual instrument. Similarly an average of the rms values of the maximum g-forces using the powered prototype was calculated. Thus, average of maximum g-forces using manual instruments in tru-trainer and cadaver was 560 while average of maximum g-forces using powered prototype in tru-trainer and cadaver was 476.55. The percentage reduction for the maximum g-forces for surgeon 1 was calculated to be 14.90%.

Table 15 shows the calculated percentage reduction of maximum G-forces, 95% die-down reduction time and work done of only the cadaver data.

Table 15: Calculated Percentage Reduction for Cadaver Data

		% Reduction (only cadavers)
Surgeon 1	Max g-force	14.90
	Die down	32.20
	Work done	16.57
Surgeon 2	Max g-force	29.12
	Die down	42.60
	Work done	16.58
Surgeon 3	Max g-force	15.23
	Die down	2.21
	Work done	10.14
Surgeon 4 (*)	Max g-force	-18.26
	Die down	33.33
	Work done	7.48
Surgeon 5	Max g-force	13.43
	Die down	24.48
	Work done	12.12

* The data of Surgeon 4 was an outlier as the data was not collected properly due to triggering problems. See Appendix E for 3Dx data

In order to compare the manual instrument and powered prototype, the average of the maximum g-forces obtained by all the 5 surgeons using the manual instruments on the cadavers in both 3Dx and G4 stations was calculated to be 532.83. For the powered prototype, the average of the maximum g-forces was calculated as 385.33. The percentage reduction in g-forces while using the powered instrument was calculated to be 27.68%. The next table provides the percentage reduction of g-forces, 95% die-down and the work done while using the powered instrument on cadavers.

Table 16: Percentage Reduction using the powered instrument

	Manual (average)	Powered (average)	% Reduction
Max g-force	532.83	385.33	27.68
95% Die-Down	0.0045173	0.002872	36.42
Work Done	0.0053	0.00463	12.64

The standard deviation for the work done using both manual and powered instrument was calculated for consistency is shown in the next table. A lower standard deviation implies more consistency.

Table 17: Standard Deviation for the Work Done

	Manual (Std. Dev)	Powered (Std. Dev)	% Reduction
Consistency of Work Done	0.00220404	0.002089	5.21

3.4 Summary for Manual / Powered Instruments Comparison

This section provided a performance comparison between a manual torquing instrument and a powered prototype used in spinal constructs in neurosurgery. The data was collected by using a specially designed fixture that is fixed to the adjoining pedicle screw and allows for the easy installation of two accelerometers. The two accelerometers provide data so that the actual vectorial g-force measurement can be made in the plane of the motion. Results are presented for both the tru-trainer and cadaver studies conducted by the five surgeons invited for the cadaver lab. The comparison study between the manual and the powered instrument are presented only for the cadavers (for purposes of claims as well as publications) though the tru-trainer data is extremely consistent, and does not change the results by much.

Given below are the final reduction numbers for the four metrics selected to show the superiority/efficacy of the powered instrument over the manual one. The summary of the Cadaver lab results are plotted in Figure 50.

- A 27.68% reduction in g-forces was observed while using the powered instrument.
- There is also a 36.42% reduction in die-down time while using the powered instrument
- A 12.64% less energy is felt on the adjoining screw.
- 5.21% reduction in the standard deviation of the work done meaning higher consistency.

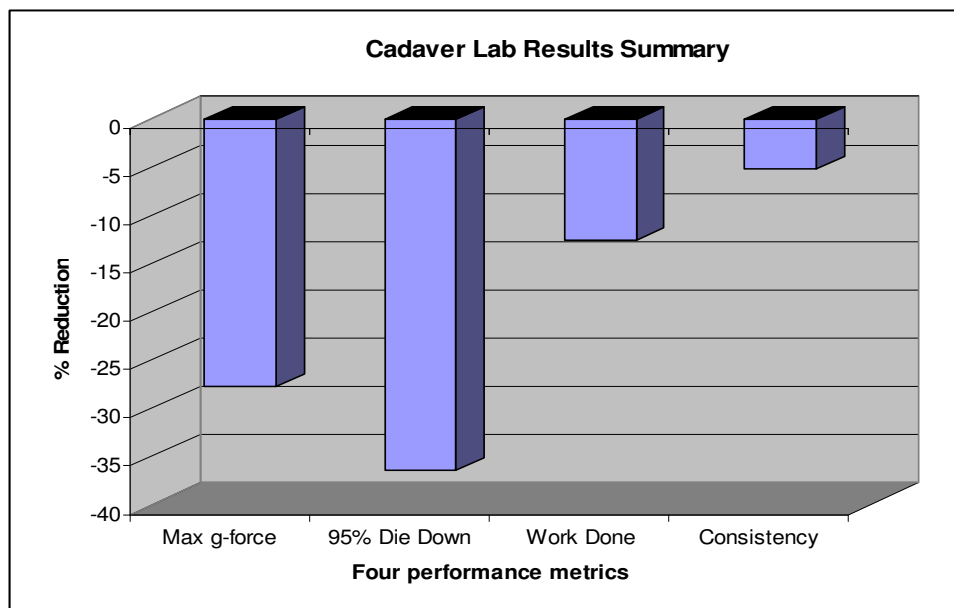


Figure 50: Cadaver Lab Results Summary

CHAPTER 4 – ONSET OF FATIGUE IN A SURGEON BASED ON BENCH RESULTS OF G-FORCE MEASUREMENTS

This section provides bench results for the measurement of neuromuscular activity in a surgeon's arm along with external g-force measurements for a short intense procedure during spinal reconstruction that may provide indicators for the onset of fatigue. Electromyography (EMG) and acceleration measurements were recorded during the event of the breaking of the set-screw head. Neuromuscular fatigue of the forearm muscles was quantified using EMG and the processing of the signals into temporal and spatial domains. Based on the g-force and torque measurements study, the external work done by the surgeon can be calculated.

Very few studies have been conducted to determine muscular activity in surgeons during surgery that results in the onset of fatigue. However, studies to examine fatigue neuromuscular changes have been conducted using electromyography.

In 1978, a study was conducted by Jonsson to show that Electromyography (EMG) was feasible to measure the force of contraction of individual muscles during prolonged work [41]. This was used to evaluate work done by utilizing threshold limits of muscular loads for continuous work.

Komi et al [42] studied fatigue of the vastus lateralis muscle in healthy students with regards to their muscle fibre type distribution. They took muscle force decline as the criterion to determine the degree of fatigue. They analyzed integrated EMG (IEMG) and Mean Power Frequency (MPF) to study the qualitative and quantitative changes. Their results found that students rich in muscles made up of Fast Twitch (FT) fibres showed higher peak knee extension torque and greater tendency to fatigue than students with muscles made up of Slow Twitch (ST) fibres.

A recent study was conducted by Uhrich et al to assess muscle activity and compared the effects of fatigue, monitor placement and surgical experience in surgeons using EMG during a simulated laparoscopic surgery [43].

This study aims at providing an in-depth analysis of the event which can be used for improved design of the spinal constructs, the instrumentation as well as ergonomic studies so as to improve procedures that benefit the surgeons.

4.1 EMG Test Set-up and Data Collection

Electromyography is a study performed to assess the health of the muscles and the nerves that control the muscles. This test is performed by inserting a needle electrode through the skin into the muscle. The electrical activity is then detected by the electrode and is displayed on an oscilloscope. The shape, size of the wave forms on the oscilloscope show the contraction of the muscle (usually done by flexing the arm) [44]. Muscle fatigue covers effects that impair motor performance. It is a response to physical exertion or force. It includes the effort to exert this force and the eventual inability to produce or maintain the force [45]. Figure 51 below shows the EMG Data Acquisition System.

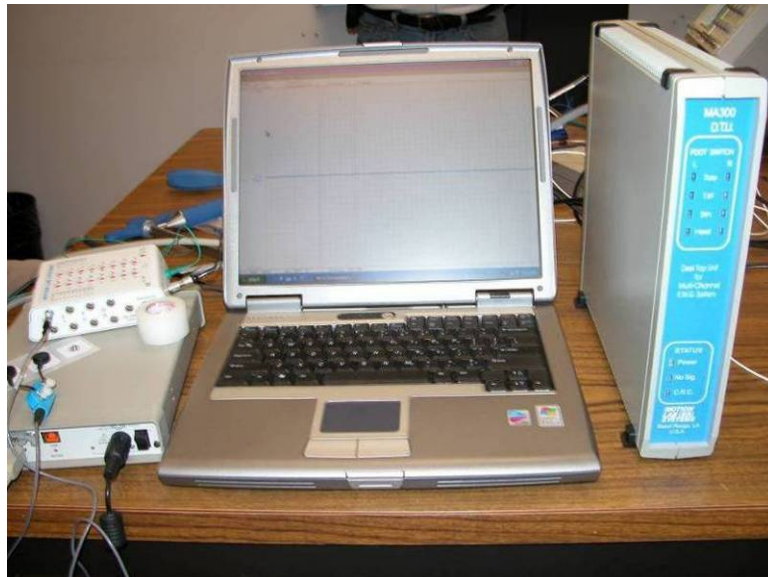


Figure 51: EMG Data Acquisition and Monitoring System

Figure 52 below shows the test set-up for EMG data acquisition.

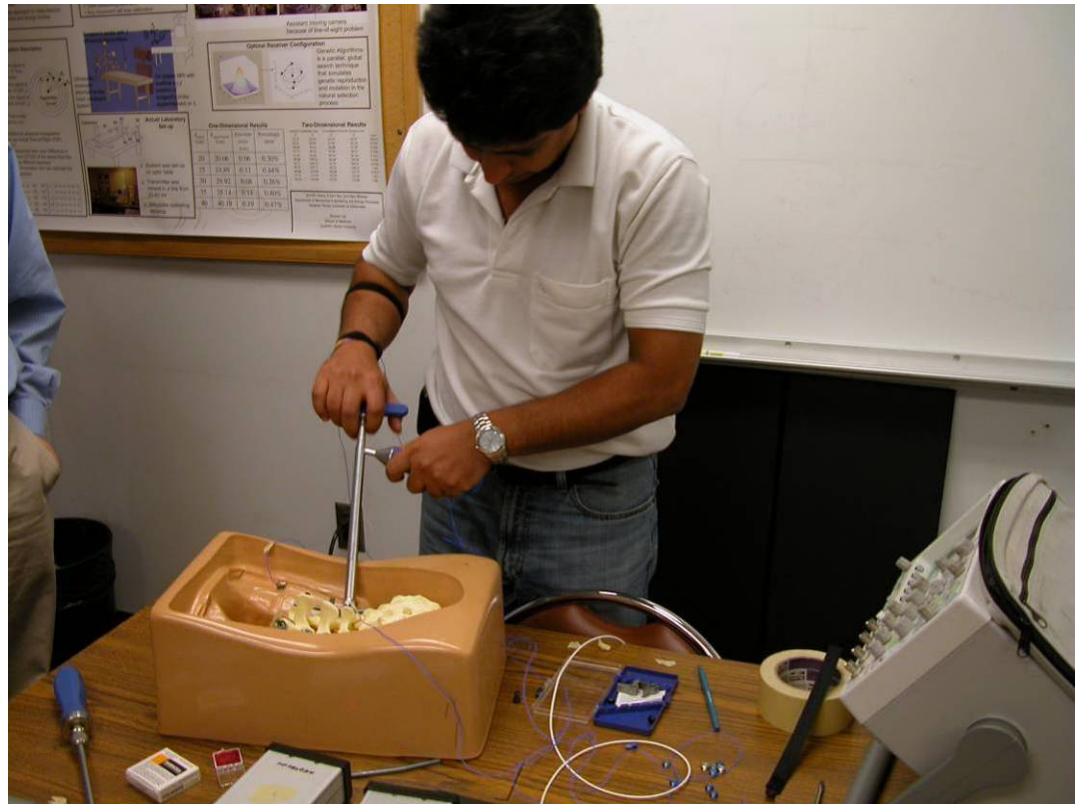


Figure 52: EMG Test Laboratory Set-up

Surface electromyography (EMG) was recorded from the flexor muscles of the right forearm (Figure 53). Bipolar, silver-silver chloride single differential gel electrodes positioned 2.0 cm center to center were aligned parallel to the length of the underlying muscle. The bandpass filter was set 20 – 500 Hz, at a CMRR of less than 90dB at 60 Hz, and signals were recorded at 4000 Hz using a 12 bit A/D converter and then stored for future analysis. Signals were pre-amplified up to 500x.

Discrete Fourier transform algorithms were used to analyze the power density spectrum of the EMG signal. These were sampled in 500 ms increments leading up to the event. Briefly, the spectrum of the EMG signal is compressed to lower frequencies as propagation of the signal is reduced due to build up of metabolic wastes in the muscles.

The raw EMG signals were rectified and further low-pass filtered at 30 Hz using a fourth-order zero-lag Butterworth filter. The signal was then segmented into 500 ms analysis windows and integrated. A combination of frequency compression and increased signal amplitude denotes neuromuscular fatigue of the general muscle group.

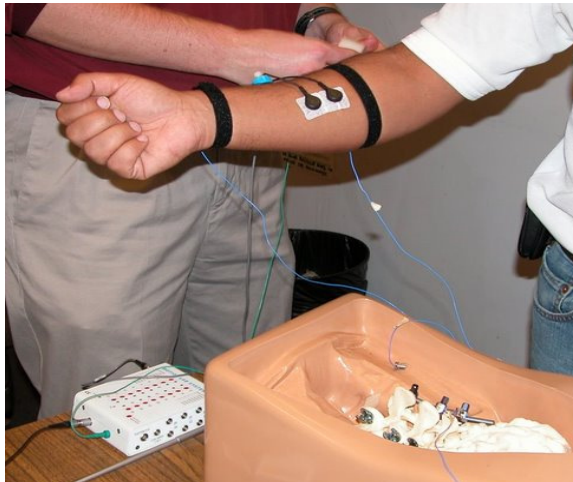


Figure 53: EMG Data Recording

4.2 Onset of Fatigue

Four set screws were torqued off in quick succession, and the time plot of the first one is shown in Figure 54. There were three additional similar events recorded by the EMG system.

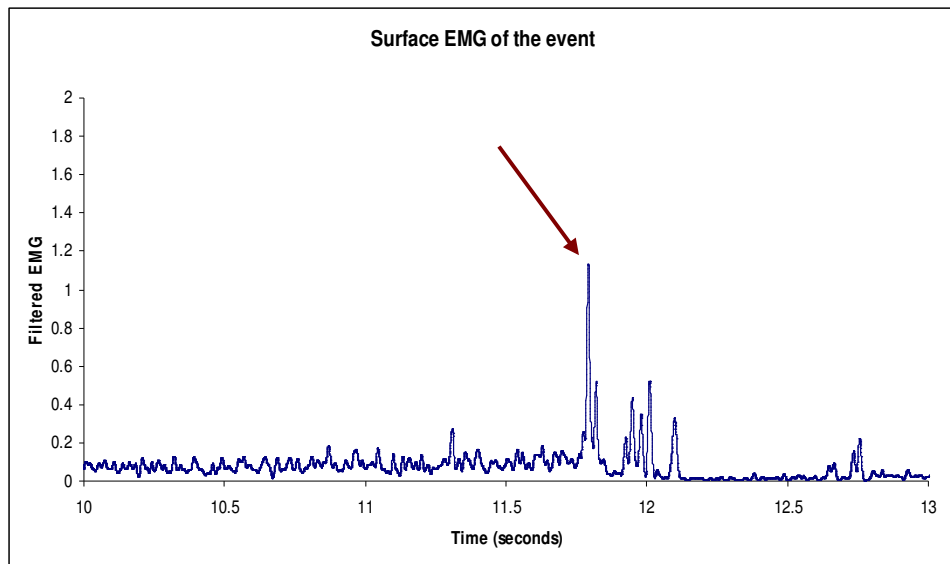


Figure 54: Surface EMG of the Event

The EMG signal recorded from the forearm was processed into a frequency domain and a spatial domain to further examine neuromuscular fatigue. Over consecutive pedicle screw torquing events the participant subjectively stated that he was tired. The data from the frequency content and integrated EMG verify this assessment as shown in Figure 55 and Figure 56.

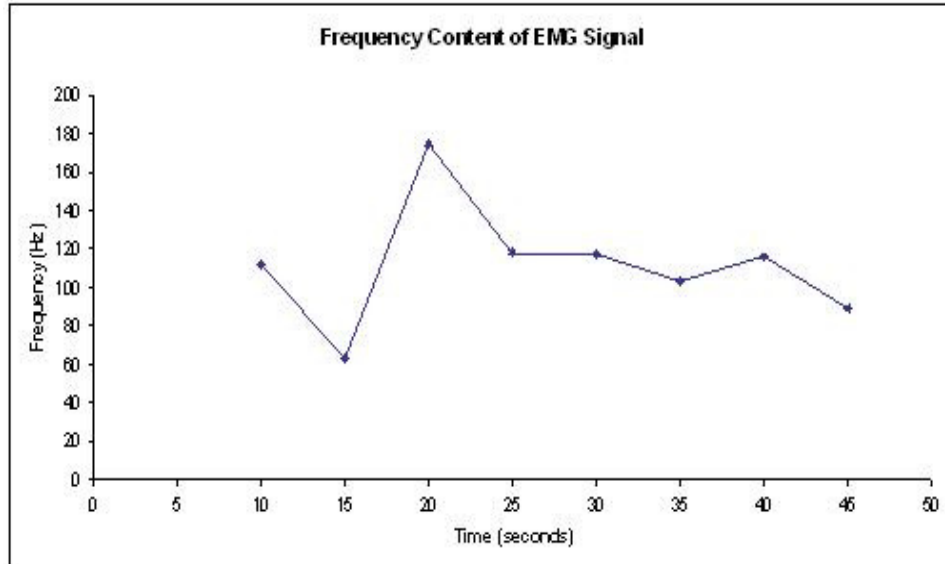


Figure 55: Median Frequency Content of the EMG Density Spectrum

Figure 55 denotes the four events (10-15 sec, 20-25 sec, 30-35 sec and 40-45 sec). It can be seen that the spectrum of the EMG signal is compressed to lower frequencies as propagation of the signal is reduced due to build up of metabolic wastes in the muscles. Notice the downward trend of all four events. A combination of frequency compression and increased signal amplitude denotes neuromuscular fatigue of the general muscle group.

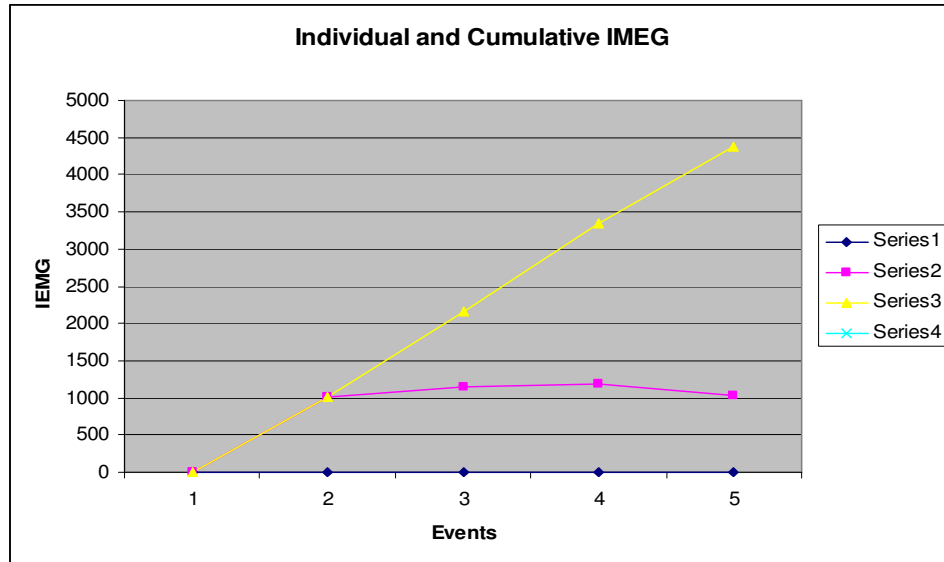


Figure 56: Integrated EMG from forearm muscles

Figure 56 shows the integrated EMG (IEMG) for each individual event as well as the cumulative IEMG from the data leading up to each of the four events. Frequency content reduction occurred in the muscle leading up to the event. Likewise, increased amplitude of the EMG signal indicates further recruitment of muscle fibers to compensate for the fatigued muscles at each event. Fatigue in the forearm muscles as evidenced by the changes in the EMG signal likely correspond to depletion of phosphagen metabolites, specifically creatine phosphate, within the muscle fibers.

To then connect this data to a quantitative fatigability study, calibration studies were conducted using a hand exercise dynamometer. Results are shown in the next section.

4.3 EMG Data Analysis

Normalized EMG plots were developed to categorize the onset of fatigue. Figures 57 – 64 show the plots EMG data series and normalized NEMG plots. This is obtained by flipping the data and normalizing it by dividing by the peak values in the data. The normalized EMG (%MVIC) is plotted on the x-axis and time is plotted on the y-axis.

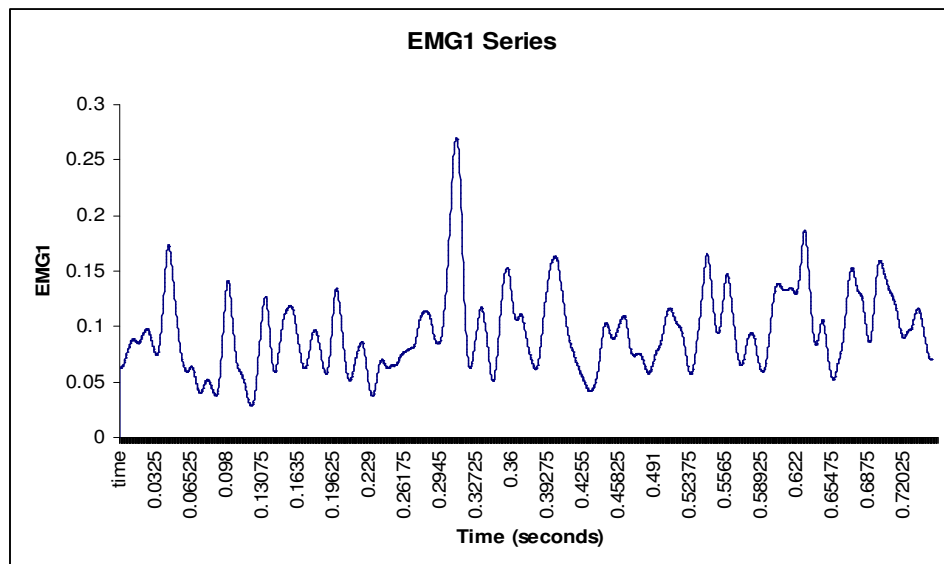


Figure 57: EMG Data Series 1

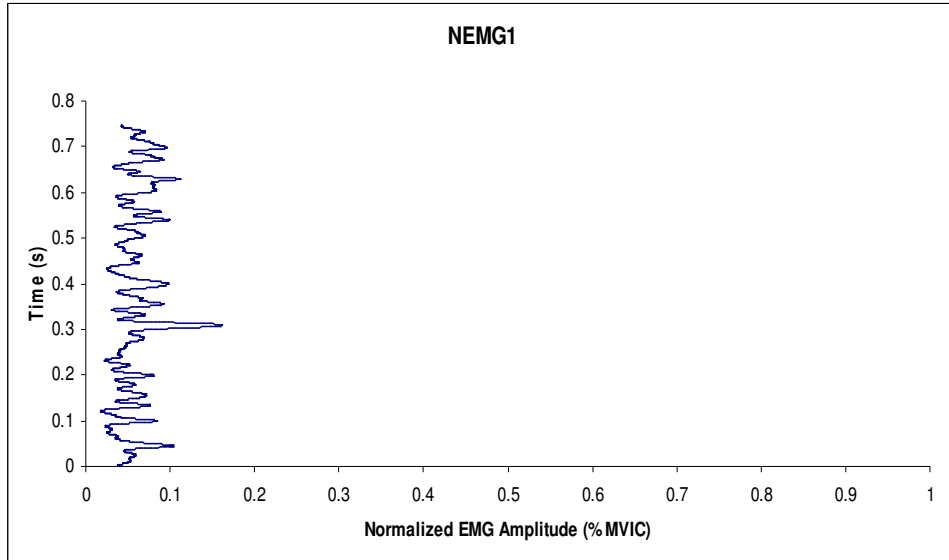


Figure 58: Normalized EMG Data Series 1

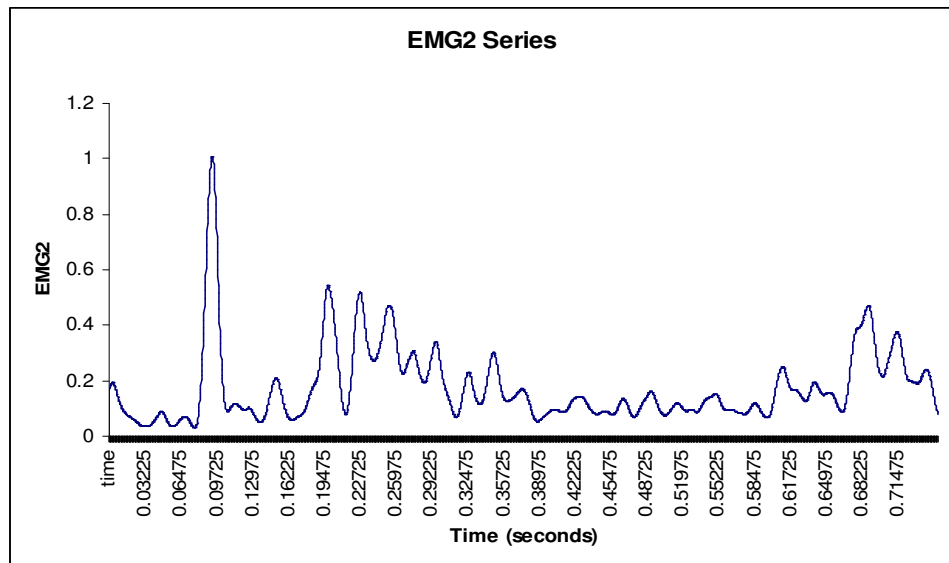


Figure 59: EMG Data Series 2

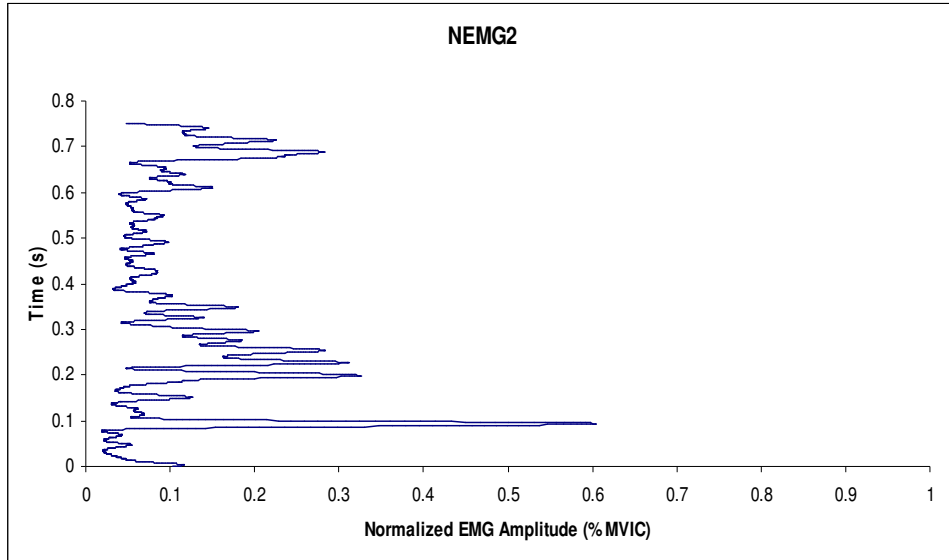


Figure 60: Normalized EMG Data Series 2

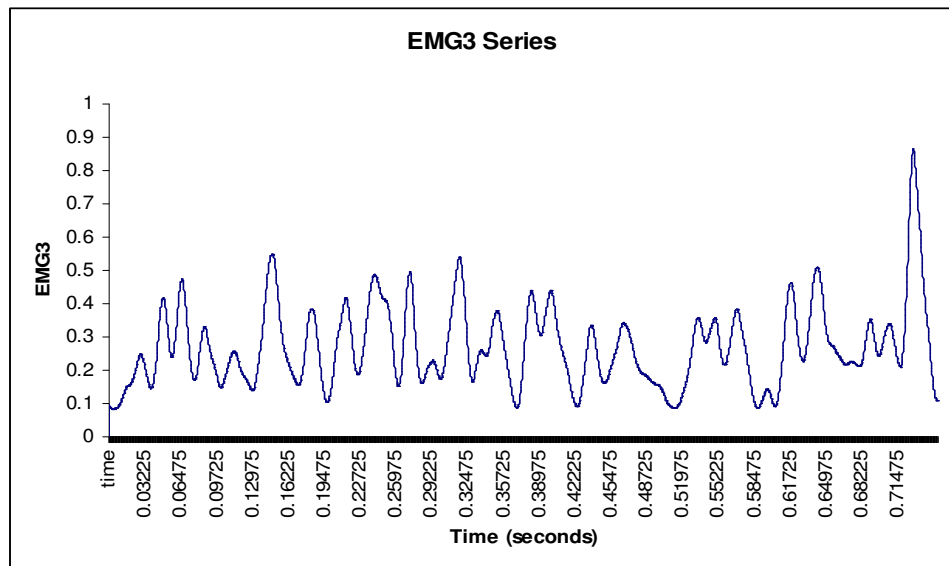


Figure 61: EMG Data Series 3

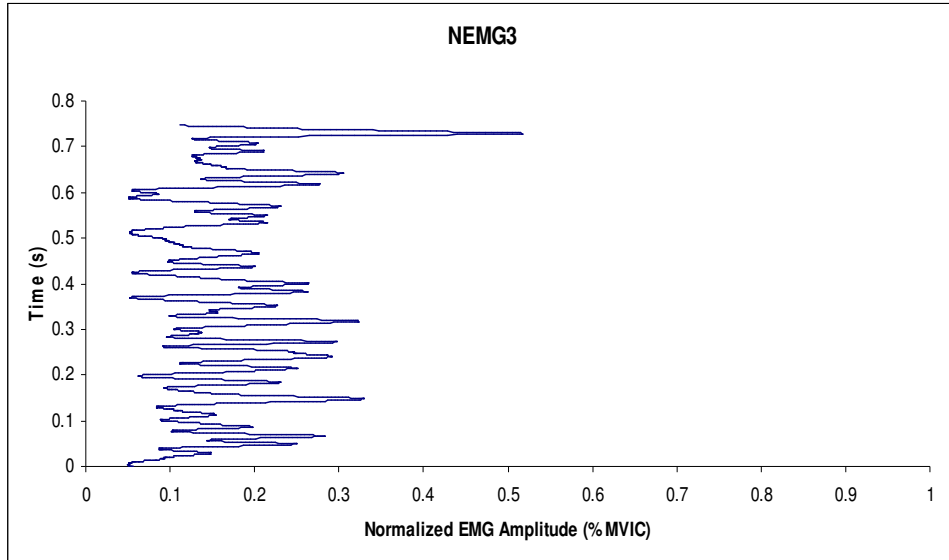


Figure 62: Normalized EMG Data Series 3

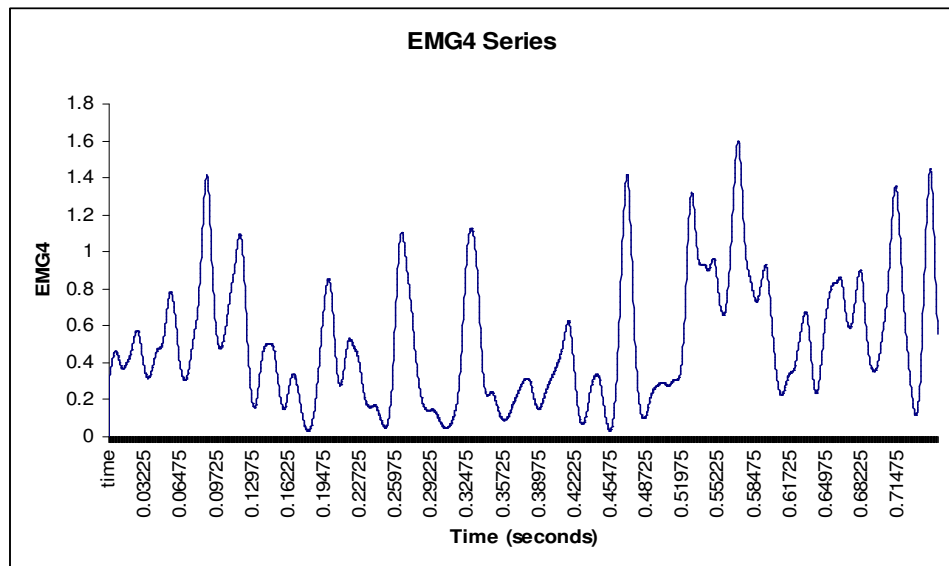


Figure 63: EMG Data Series 4

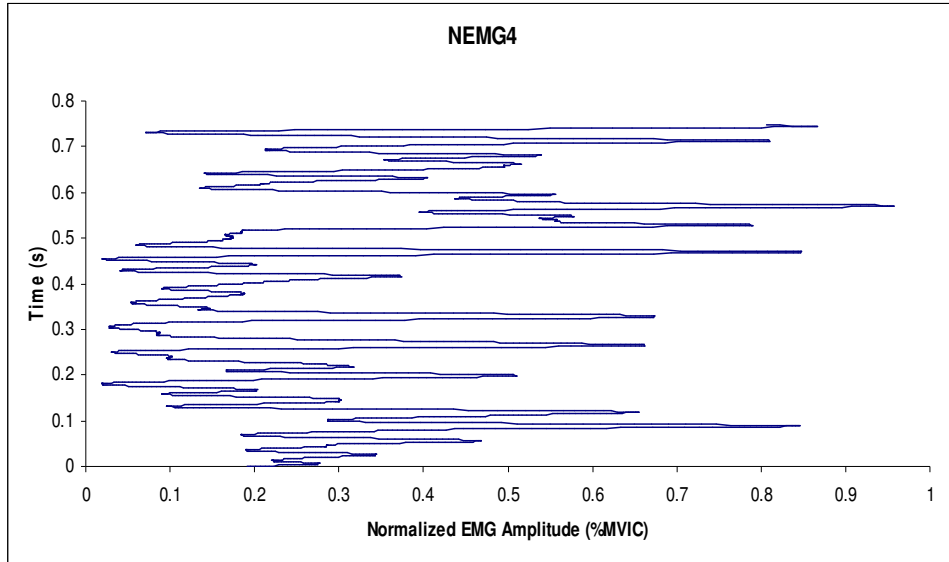


Figure 64: Normalized EMG Data Series 4

Figure 65 shows the probability chart for all four events (blue, red, green, and gray lines represent the EMG1, EMG2, EMG3, and EMG4, respectively). Many aspects of this current chart are similar to the ones shown in Jonsson (41). The overall MVC% plot is shown below:

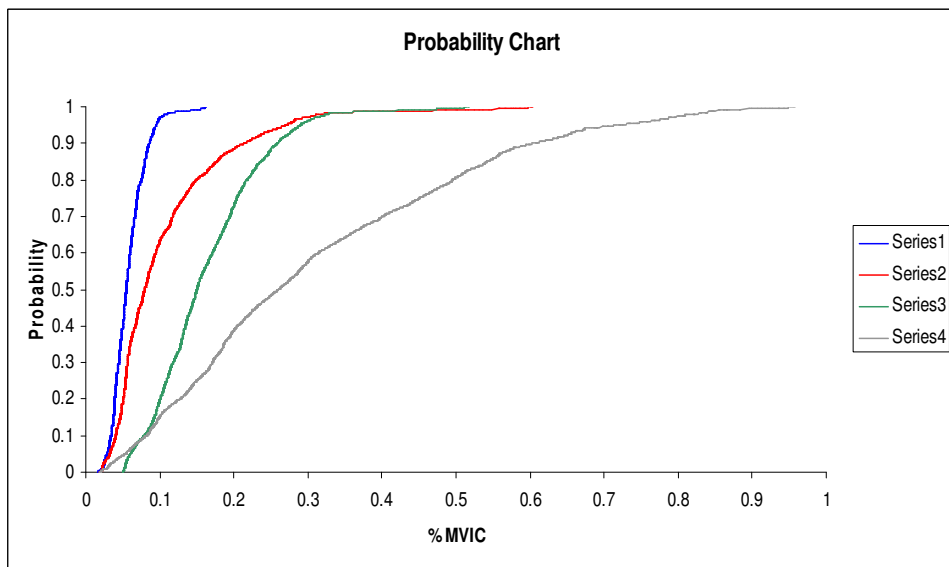


Figure 65: Probability Chart showing Fatigability

4.4 Summary on Onset of Fatigue Study

This section discussed the acceleration measurements taken on the spinal construct as well as the surgeon's wrist and elbow during the event of the breaking of the set-screw head. This event which happens in about 50-100 microseconds, showed almost 25g's being recorded on the surgeon's wrist and elbow. Based on previous work done on G-force and torque measurements that shows that the torque required is 12 Nm, the external work done by the surgeon was calculated to be about 60-120 KJ. The onset of fatigue was apparent in consecutive break events as illustrated by the change in EMG parameters over time. Events 1, 2, 3 and 4 are shown in Figure 65, and they all show a movement downwards and to the right. Such a trend indicates too high a muscular load when using a heavy tool (3 and 4). But since the tool being used is the same, it must imply that extra effort is being put in to the event by the surgeons. Events 1 and 2 are acceptable from a fatigability point of view, but 3 and 4 definitely show onset of fatigue. Event 3 could imply too high a static load, but then get slightly better, while event 4 is too high a static load and peak load. All of these interpretations are based on the work done by Johnsson (41).

CHAPTER 5 – CONCLUSIONS AND RECOMMENDATIONS

There were basically three main purposes in this research study. They were:

- Measurements of G-forces and torque during set-screw break-off.
- Comparison of manual and neurosurgical powered torquing instruments.
- Onset of fatigue in a surgeon based on G-force measurements.

The results from the tests conducted on g-force and torque measurements were promising. The data from the set screws being torqued off using the manual instrument showed high g-forces consistently and accurately, in the range of 400-800g's. The measurements were also verified by using 3 high speed cameras from different companies which gave similar g-force values. The TEMA software used in the high speed camera image analysis calculation showed capability in giving distinct results on the displacement, velocity and acceleration. The acceleration plots obtained from using this software were correlated with the accelerometer measurements and were found to be very similar. The value of the torque obtained from Distortion Energy Theory for material fracture was 12.26 N-m and it was 12.28 N-m from the Fully Plastic Torque calculations. Measurements using a torque wrench gave the value of torque as 11.30 N-m. These torque values closely matched the design torque provided by Medtronic which was 11.00 N-m.

The data obtained from the first part of this study was subsequently used in the performance comparison of the manual torquing instruments with a newly introduced powered prototype. This study was not conducted at SIUC and the tests were performed by surgeons operating on tru-trainers and cadavers. These tests were mainly conducted to show that the powered prototype is more effective in reducing g-forces on the implant and ultimately on the spine.

The break-off tests using manual and powered torquing instruments were performed on both tru-trainer and cadavers and the data sets obtained for all these sets were analyzed. However, more importance was given to the data sets obtained for the cadaver experiments. Table 16 in chapter 4 provides the performance comparison of both manual and torquing instruments on cadavers. The results were fairly conclusive in achieving the objectives of this study. The results clearly indicated that using the powered prototype reduces the effect of g-forces on the implant by as much as 27.68%. The effect of torquing of a single set-screw on the subsequent screws was also reduced with the die-down time value coming up to be around 36.42% and the energy felt on the adjacent screws was 8.52% less. A 5.21% reduction in the standard deviation was calculated to show the consistency in using the powered instruments. Figure 66 provides a 3-dimensional comparison of the 5 surgeons in terms of percentage reduction of the maximum g-forces, 95% die –down and work done (or energy).

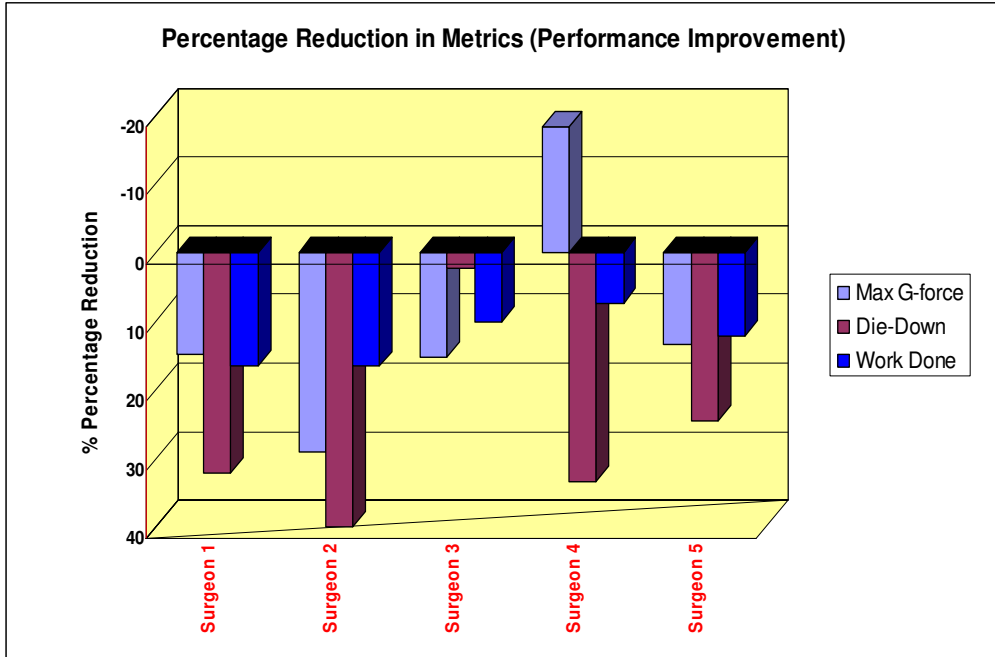


Figure 66: Performance Comparison of the 5 Surgeons

The third part of this project was conducted in order to show that the complexity and the length of these surgical procedures affected the surgeons eventually leading to fatigability. It is difficult to quantify the exact chemical energy expenditure as this will be specific to each individual; however, this study showed that work on a multi-level construct influences the subsequent performance of the surgeon. Based on the results of the previous studies, the external work done by the surgeon was calculated to be between 60 to 120 KJ. The EMG test results showed that the onset of fatigue was noticeable. The result of this study is important as no previous studies have been conducted to determine fatigability in a surgeon.

The current facilities at the SIUC Engineering Building support conducting experiments on g-force and torque measurements using accelerometers, DIC and torque wrenches. Facilities are also available for conducting fatigability tests at the Department of Kinesiology, SIUC. These facilities have shown the capability of providing accurate results based on the number of experiments conducted. However, in the scope of this study, some of the facilities can be improved and a few recommendations are:

- Equip the laboratory with the purchase of high-speed camera.
- The tests conducted at SIUC did not include the influence of the saw bone structure. Tests could be performed to determine the effect of this structure on the g-force and torque measurements. Also, investigate other methods to measure g-forces and torque. Better fixtures can be designed to hold the accelerometers.
- A powered prototype can be obtained to perform some of these tests.
- Investigate methods other than EMG measurement to determine onset of fatigue.
- Investigate sources of error, if any, due to experimental setup, instrumentation and data acquisition systems.

This research was conducted using top-loading connectors consisting of pedicle screws and rods made of Titanium alloy Ti6Al4V. Current state-of-the-art products such as CD HORIZON® LEGACY™ PEEK Rod System have been

introduced by Medtronic Sofamor Danek into the market. This particular product makes use of a biomaterial called Polyetheretherketone, more commonly known as PEEK. PEEK is a unique biocompatible and stable polymer with a semi-crystalline structure. It has excellent thermal, chemical, and combustion properties critical to performance and is ideally suited for in vivo medical device applications as it combines outstanding chemical and hydrolysis resistance, high strength and excellent tribological properties with extensive biocompatibility. It has a high melting temperature (~343 °C), glass transition temperature (~145 °C) and high chemical resistance [46]. Unreinforced PEEK has a Young's modulus of 3.6GPa. Addition of short biocompatible carbon fibers can increase the young's modulus from 3.6GPa up to 7.44GPa for 30% GF-PEEK and 12.38GPa for 30% CF-PEEK [47]. Various studies have been conducted successfully on PEEK being used as an implant material. As part of future research at SIUC, the existing titanium alloy implants can be replaced by the PEEK implant. Finite Element studies can be conducted as part of this study.

REFERENCES

- [1] Pullout Strength of Pedicle Screws versus Pedicle and Laminar Hooks in the Thoracic Spine. Liljenqvist U, Hackenberg L, Link T, Halm H. 2001 Apr; 67(2):157-63.
- [2] Website: <http://www.spineuniverse.com/displayarticle.php/article2000.html>, February 24, 2009.
- [3] Website: <http://www.back.com/anatomy.html>, February 24, 2009.
- [4] Website: <http://www.emedicine.com/neuro/topic657.htm>, February 24, 2009.
- [5] Website: <http://www.apparelyzed.com/spinalcord.html>, February 24, 2009.
- [6] Website: <http://www.spineuniverse.com/displayarticle.php/article1267.html>, February 24, 2009.
- [7] Website: <http://www.innerbody.com/image/skel05.html#>, February 24, 2009.
- [8] Website: <http://www.spineuniverse.com/displayarticle.php/article2000.html>, February 24, 2009.
- [9] Website: http://wwwp.medtronic.com/Newsroom/LinkedItemDetails.do?itemId=1101754369520&itemType=backgrounder&lang=en_US, February 24, 2009
- [10] Website: http://www.chirogeek.com/000_Disc_Anatomy.htm, February 24, 2009.
- [11] Website: http://www.neurosurgerytoday.org/what/patient_e/herniated.asp, February 24, 2009.
- [12] Website: <http://www.spinalstenosis.org/definition.php>, February 24, 2009.
- [13] Website: <http://www.nyp.org/health/adult-spinal-deformity.html>, February 24, 2009.
- [14] Website: <http://www.netwellness.org/healthtopics/spinal/spineconditions.cfm>, February 24, 2009.
- [15] Hadra, B. E.: Wiring the spinous processes in Pott's disease. Trans. Am. Orthop. Assn., 4: 206, 1891.
- [16] King, D.: Internal fixation for lumbosacral fusion. J. Bone and Joint Surg., 30-A: 560-565, July 1948.

- [17] Harrington, P. R., and Tullos, H. S.: Reduction of severe spondylolisthesis in children. Southern Med. J., 62: 1-7, 1969.
- [18] Cotrel, Y.; Dubousset, J.; and Guillaumat, M.: New universal instrumentation in spinal surgery. Clin. Orthop., 227: 10-23, 1988.
- [19] Dick, W.: The "fixateur interne" as a versatile implant for spine surgery. Spine, 12: 882-900, 1987.
- [20] Roy-Camille, R.; Saillant, G.; and Mazel, C.: Internal fixation of the lumbar spine with pedicle screw plating. Clin. Orthop., 203: 7-17, 1986.
- [21] Roy-Camille, R.; Saillant, G.; and Mazel, C.: Plating of thoracic, thoracolumbar, and lumbar injuries with pedicle screw plates. Orthop. Clin. North America, 17: 147-159, 1986.
- [22] Louis, R.: Fusion of the lumbar and sacral spine by internal fixation with screw plates. Clin. Orthop., 203: 18-33, 1986.
- [23] Website: <http://www.fcginstitute.com/assets/docs/PedScrewCaseHistory.pdf>, February 24, 2009.
- [24] M. Aebi, J. S. Thalgott, J. K. Webb, "AO ASIF Principles in Spine Surgery," Springer, 1st edition, 1998, pp. 5-6.
- [25] Moore, Douglas C. MS., Maitra, Ranjan S. MD., Farjo, Laith A. MD., Graziano, Gregory P. MD., Goldstein, Steven A. PhD., 1997, "Restoration of Pedicle Screw Fixation With an in Situ Setting Calcium Phosphate Cement", Journal of Biomechanics Volume 22(15), pp 1696-1705.
- [26] Hirano, Toru MD., Hasegawa, Kazuhiro MD., Takahashi, Hideaki E. MD., Uchiyama, Seiji MD., Hara, Toshiaki PhD., Washio, Toshikatsu MSc., Sugiura, Toru MSc., Yokaichiya, Motoo MSc., Ikeda, Masayuki MSc., 1997, "Structural Characteristics of the Pedicle and Its Role in Screw Stability", Spine, 22(21), pp 2504-2510.
- [27] Jones, E. Ladd MD., Heller, John G. MD., Silcox, D. Hal MD., Hutton, William C. DSc., 1997, "Cervical Pedicle Screws Versus Lateral Mass Screws: Anatomic Feasibility and Biomechanical Comparison.", Spine, 22(9), pp 977-982.
- [28] Website: <http://www.visionresearch.com>, February 24, 2009.
- [29] Website: <http://www.highspeedimaging.com>, February 24, 2009.

- [30] Website: <http://www.olympusindustrial.com>, February 24, 2009.
- [31] Website:
http://www.photosonicsinternational.co.uk/software/TEMA_Software.htm,
February 24, 2009.
- [32] Shigley and Mische, "Mechanical Engineering Design," McGraw Hill, 5th edition, 2002, pp. 252-253.
- [33] Budynas, Richard G., Nisbett, Keith J., "Mechanical Engineering Design", Eighth Edition, pp 213-217
- [34] Boresi and Schmidt, "Advanced Mechanics of Materials," John Wiley & Sons, Inc, 6th edition, 2003, pp. 243-254
- [35] Website:
http://www.sears.com/shc/s/p_10153_12605_00944593000P?mv=rr, Sears Catalogue® ©, February 24, 2009.
- [36] Ganesh Gautham, Yi-Cheng Pan, Jarlen Don, Tsuchin Chu, Ajay Mahajan and Steve Summy (Medtronic), 2008, "Bench Results on G-force Measurements in a Spinal Construct during Manual Breaking off of Set Screws".
- [37] Weisner, L., Kothe, R., Ruther, W., 1999, "Anatomic evaluation of two different techniques for the percutaneous insertion of pedicle screws in the lumbar spine", Spine, 24(15), pp. 1599-1603.
- [38] Elliot, Michael J., Slakey, Joseph B., 2007, "Thoracic pedicle screw placement: Analysis using anatomical landmarks without image guidance", Journal of Pediatric Orthopedics, 27(5), pp. 582-586.
- [39] Jackson, Roger P., 1999, "Tools for Use in Installing Osteosynthesis Apparatus Utilizing Set Screw Break-off Head", U.S. Patent 5941885.
- [40] Chao, Nam T., Rybicki, Chris and Whipple, Dale, 2004, "Instrument for Inserting, Adjusting and Removing Pedicle Screws and Other Orthopedic Implants", U.S. Patent 7226453.
- [41] Jonsson, B., 1978, "Quantitative Electromyographic Evaluation of Muscular Load during Work", Scandinavian journal of rehabilitation medicine, 6, pp. 69-74.
- [42] Komi, Paavo V., Tesch, Per., 1979, "EMG Frequency Spectrum, Muscle Structure and Fatigue during Dynamic Contractions in Man", European Journal of Applied Physiology, 42, pp. 41-50.

[43] Uhrich, M. L., Underwood, R. A., Standeven, J. W., Soper, N. J., Engsborg, J. R., 2002, "Assessment of Fatigue, Monitor Placement, and Surgical Experience during Simulated Laparoscopic Surgery", Surgical Endoscopy, 16(4), pp. 635-639.

[44] Website: <http://www.nlm.nih.gov/MEDLINEPLUS/ency/article/003929.htm>, February 24, 2009.

[45] Cooper, R.G., Edwards, R. H., Gibson, H., Stokes, M. J., 1988, "Human Muscle Fatigue: Frequency Dependence of Excitation and Force Generation", Journal of Physiology, 397, pp. 585-599.

[46] Wang, C., Ma, J., and Cheng W., 2003, "Formation of Polyetheretherketone Polymer Coating by Electrophoretic Deposition Method", Surface and Coating Technology, 173(2-3), pp. 271-275.

[47] Wang, M., Porter, D., and Bonfield, W., 1994, "Processing, Characterization, and Evaluation of Hydroxyapatite Reinforced Polyethylene Composites", British Ceramics Transactions, 93(3), pp. 91-95.

APPENDICES

APPENDIX A – Sample Data (30 sets)

Time (s)	Voltage 1 (mV)	Voltage 2 (mV)	(Voltage 1) ²	(Voltage 2) ²	Average	RMS
-0.0065	-0.0620	-0.1245	0.0038	0.0155	0.0097	0.0983
-0.0065	-0.1245	-0.1245	0.0155	0.0155	0.0155	0.1245
-0.0065	-0.0620	-0.1245	0.0038	0.0155	0.0097	0.0983
-0.0064	-0.0620	0.0005	0.0038	0.0000	0.0019	0.0438
-0.0064	-0.0620	-0.1245	0.0038	0.0155	0.0097	0.0983
-0.0064	-0.0620	-0.1245	0.0038	0.0155	0.0097	0.0983
-0.0064	-0.0620	-0.1245	0.0038	0.0155	0.0097	0.0983
-0.0064	-0.0620	-0.1245	0.0038	0.0155	0.0097	0.0983
-0.0063	-0.0620	-0.1245	0.0038	0.0155	0.0097	0.0983
-0.0063	-0.0620	-0.1245	0.0038	0.0155	0.0097	0.0983
-0.0063	-0.0620	-0.1245	0.0038	0.0155	0.0097	0.0983
-0.0063	-0.0620	-0.1245	0.0038	0.0155	0.0097	0.0983
-0.0063	-0.0620	-0.1245	0.0038	0.0155	0.0097	0.0983
-0.0062	0.0005	-0.0620	0.0000	0.0038	0.0019	0.0438
-0.0062	-0.0620	-0.1245	0.0038	0.0155	0.0097	0.0983
-0.0062	-0.1245	-0.0620	0.0155	0.0038	0.0097	0.0983
-0.0062	-0.0620	-0.1245	0.0038	0.0155	0.0097	0.0983
-0.0061	-0.0620	-0.1245	0.0038	0.0155	0.0097	0.0983
-0.0061	0.0005	-0.1245	0.0000	0.0155	0.0078	0.0880
-0.0061	-0.0620	-0.1245	0.0038	0.0155	0.0097	0.0983
-0.0061	-0.0620	-0.1245	0.0038	0.0155	0.0097	0.0983
-0.0060	-0.0620	-0.0620	0.0038	0.0038	0.0038	0.0620
-0.0060	-0.0620	-0.1245	0.0038	0.0155	0.0097	0.0983
-0.0060	-0.0620	-0.1245	0.0038	0.0155	0.0097	0.0983
-0.0060	-0.0620	-0.1245	0.0038	0.0155	0.0097	0.0983
-0.0060	-0.0620	-0.1245	0.0038	0.0155	0.0097	0.0983
-0.0059	-0.0620	-0.1245	0.0038	0.0155	0.0097	0.0983
-0.0059	-0.0620	-0.1245	0.0038	0.0155	0.0097	0.0983
-0.0059	-0.0620	-0.1245	0.0038	0.0155	0.0097	0.0983
-0.0059	-0.0620	-0.1245	0.0038	0.0155	0.0097	0.0983
-0.0058	-0.0620	-0.1245	0.0038	0.0155	0.0097	0.0983
-0.0058	-0.0620	-0.0620	0.0038	0.0038	0.0038	0.0620

APPENDIX B – Equipment Specifications

Kistler Accelerometer:

Make:	Kistler
Type:	8728A500
Measuring range:	+/- 500g
Transverse sensitivity:	0.5%
Sensitivity:	10.68 mV/g
Resonant frequency:	76.0 kHz
Temperature range:	54 – 120 °C.

Oscilloscope:

Make:	Agilent Technologies
Model:	54624 A
Bandwidth:	100 MHz
Max. Sampling Rate:	200 MSa/s
Max. Memory:	4 MB
Channels:	4

Torque Wrench:

Make:	Craftsman Microtork® Torque Wrench
Item Weight:	1.7 lbs
Wrench Type:	Torque
Torque Drive Size:	3/8 in.
Torque Increments:	1.0 in. lbs.
Torque Measure:	25 to 250 in. lbs.

Vision Research Camera Specifications:

Type: Phantom V73

- 6242 frames-per-second
- 1280x800 "widescreen" resolution
- 1,000,000 pictures-per-second at reduced resolution

Motion Engineering Camera Specifications:

Type: Photron FASTCAM Ultima

- 1,024 by 1,024 pixel resolution at 3,000 frames-per-second.
- 512 by 512 pixels at 10,000 frames-per-second.
- 64 x 64 pixels at 250,000 frames-per-second.

Olympus Camera Specifications:

Type: Olympus i-speed 3

- Full resolution recording to 2,000 fps.
- 150,000 frames-per-second at maximum record speed.

MA-300 Specifications:

- 6 EMG channels (DC to 2,000Hz -3dB),
- Individual gain calibration and signal level indicator.
- Four "research" channels (DC to 120Hz, -3dB), suitable for EKG, goniometers, and pressure sensors, etc.
- Eight switch contact channels for events such as foot contact etc.

MA-720 Specifications:

- 16 channel real-time EMG display software (WinDaq/Lite).
- 32 single-ended or 16 differential analog input channels.
- Internal sampling rates up to 250 kHz at 16-bit resolution.
- Input range ± 1.25 to $\pm 10V$.
- Four programmable gain selections (1, 2, 4, 8).
- Interface via USB (recommended) or EPP parallel port.
- Small size - 9" x 7.29" x 1.52" (L x W x H).

Bandpass Filter Specifications:

- 300-2200 Hz. Low Pass Integrated Band Pass Filter.

Dynamometer Specifications:

- Baseline 300 lb. / 135kg. dial dynamometer
- 12-0246 - large dial gauge

Material – Titanium Alloy:

The implant used in the study is constructed out of Titanium Ti-6Al-4V grade 5 alloy. It is an alpha-beta alloy and is fully heat treatable. It has an excellent biocompatibility when contact with tissue or bone is required [51]. Table 19 shows the components in a Ti-6Al-4v grade 5 alloy and their percentage by weight.

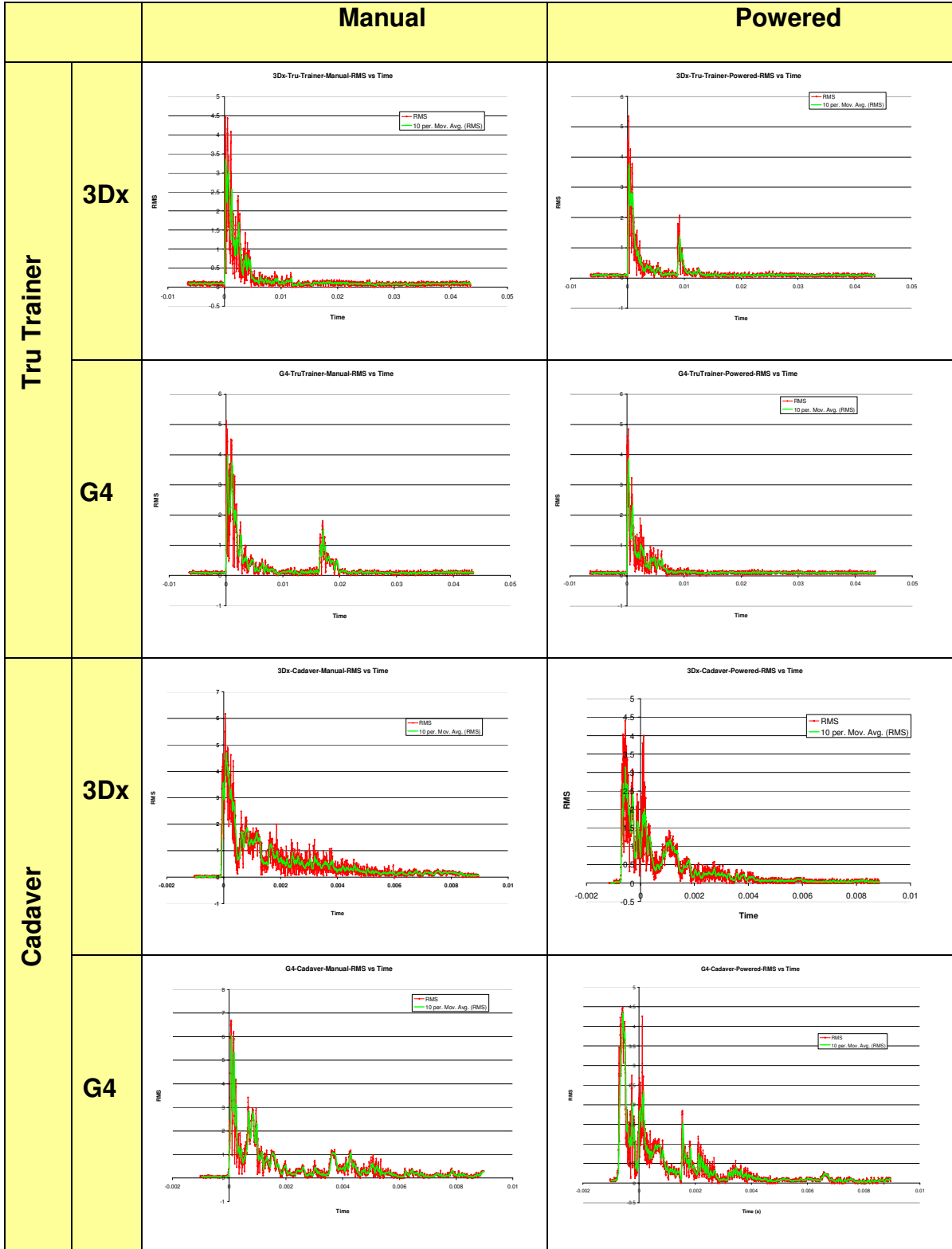
Table 18: Components of Titanium Alloy Ti-6Al-4V [51]

Component	Weight (%)
Carbon, C	< 0.08%
Iron, Fe	< 0.25%
Nitrogen, N ₂	< 0.05%
Oxygen, O ₂	< 0.2%
Aluminum, Al	5.5 – 6.76%
Vanadium, V	3.5-4.5%
Titanium	Balance

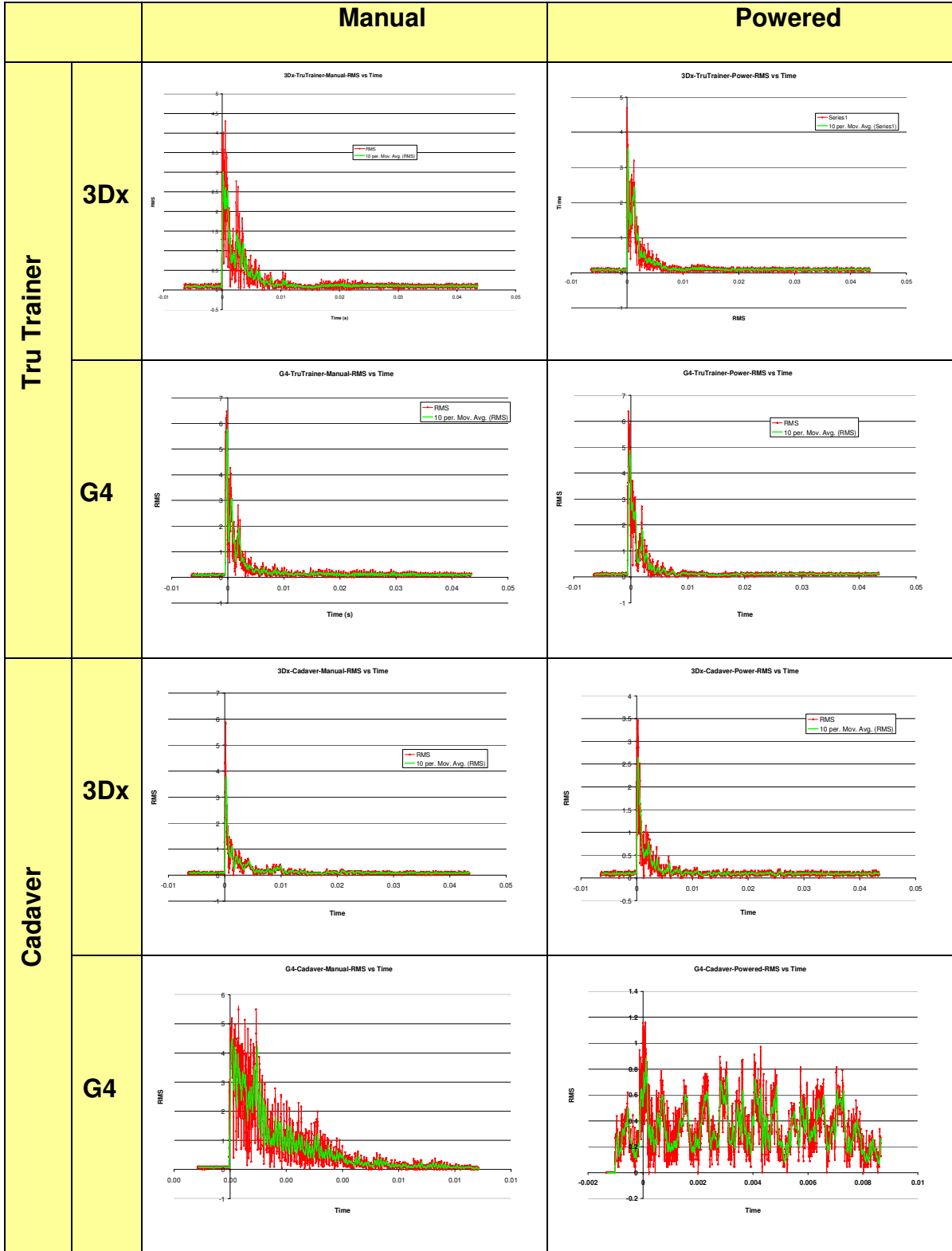
APPENDIX C – Raw Data from Surgeon 1

		Manual	Powered
Tru Trainer	3Dx	<p>3Dx-TruTrainer-Manual-RMS vs Time</p>	<p>3Dx-TruTrainer-Power-RMS vs Time</p>
	G4	<p>G4-TruTrainer-Manual-RMS vs Time</p>	<p>G4-TruTrainer-Power-RMS vs Time</p>
Cadaver	3Dx	<p>3Dx-Cadaver-Manual-RMS vs Time</p>	<p>3Dx-Cadaver-Power-RMS vs Time</p>
	G4	<p>G4-Cadaver-Manual-RMS vs Time</p>	<p>G4-Cadaver-Powered-RMS vs Time</p>

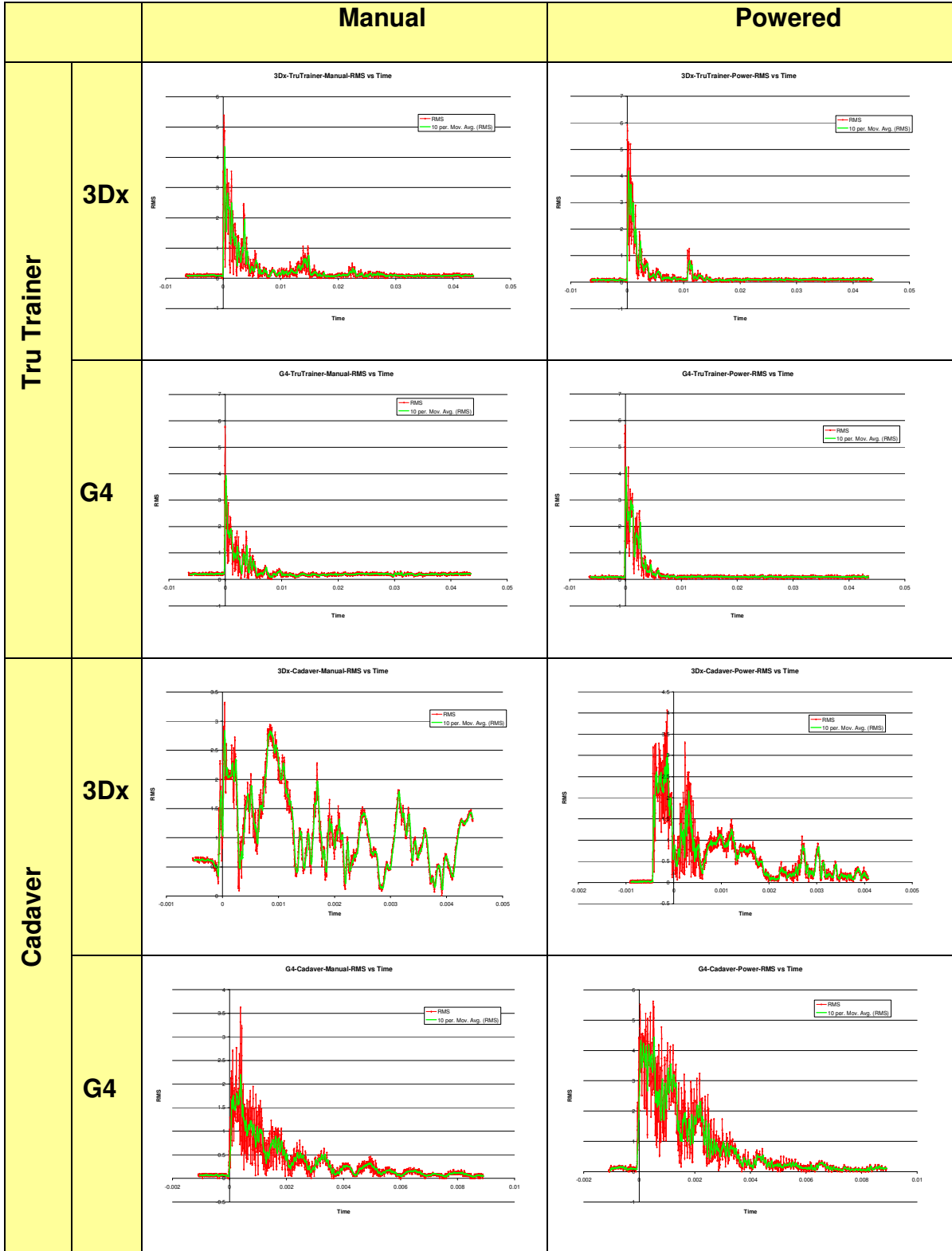
APPENDIX D – Raw Data from Surgeon 2



APPENDIX E – Raw Data from Surgeon 3



APPENDIX F – Raw Data from Surgeon 4



APPENDIX G – Raw Data from Surgeon 5

		Manual	Powered
Tru Trainer	3Dx	<p>3Dx-TruTrainer-Manual-RMS vs Time</p> <p>This graph shows RMS (Root Mean Square) on the y-axis (ranging from -0.01 to 0.05) against Time on the x-axis (ranging from -0.01 to 0.05). Two data series are plotted: RMS (red line) and 10 per. Mov. Avg. (RMS) (green line). Both series show a sharp initial peak at time 0, followed by a rapid decay to a low, stable baseline.</p>	<p>3Dx-TruTrainer-Power-RMS vs Time</p> <p>This graph shows RMS (Root Mean Square) on the y-axis (ranging from -0.01 to 0.05) against Time on the x-axis (ranging from -0.01 to 0.05). Two data series are plotted: RMS (red line) and 10 per. Mov. Avg. (RMS) (green line). The initial peak is significantly higher than in the manual mode, and the decay to the baseline is slower.</p>
	G4	<p>G4-TruTrainer-Manual-RMS vs Time</p> <p>This graph shows RMS (Root Mean Square) on the y-axis (ranging from -0.01 to 0.05) against Time on the x-axis (ranging from -0.01 to 0.05). Two data series are plotted: RMS (red line) and 10 per. Mov. Avg. (RMS) (green line). The initial peak is sharp and decays quickly to a low baseline.</p>	<p>G4-TruTrainer-Power-RMS vs Time</p> <p>This graph shows RMS (Root Mean Square) on the y-axis (ranging from -0.01 to 0.05) against Time on the x-axis (ranging from -0.01 to 0.05). Two data series are plotted: RMS (red line) and 10 per. Mov. Avg. (RMS) (green line). The initial peak is higher than in manual mode, and the decay is slower.</p>
Cadaver	3Dx	<p>3Dx-Cadaver-Manual-RMS vs Time</p> <p>This graph shows RMS (Root Mean Square) on the y-axis (ranging from -0.002 to 0.01) against Time on the x-axis (ranging from -0.002 to 0.01). Two data series are plotted: RMS (red line) and 10 per. Mov. Avg. (RMS) (green line). The initial peak is sharp and decays quickly to a low baseline.</p>	<p>3Dx-Cadaver-Power-RMS vs Time</p> <p>This graph shows RMS (Root Mean Square) on the y-axis (ranging from -0.002 to 0.01) against Time on the x-axis (ranging from -0.002 to 0.01). Two data series are plotted: RMS (red line) and 10 per. Mov. Avg. (RMS) (green line). The initial peak is much higher than in manual mode, and the decay is significantly slower, with more oscillations.</p>
	G4	<p>G4-Cadaver-Manual-RMS vs Time</p> <p>This graph shows RMS (Root Mean Square) on the y-axis (ranging from -0.002 to 0.01) against Time on the x-axis (ranging from -0.002 to 0.01). Two data series are plotted: RMS (red line) and 10 per. Mov. Avg. (RMS) (green line). The initial peak is sharp and decays quickly to a low baseline.</p>	<p>G4-Cadaver-Power-RMS vs Time</p> <p>This graph shows RMS (Root Mean Square) on the y-axis (ranging from -0.001 to 0.005) against Time on the x-axis (ranging from -0.001 to 0.005). Two data series are plotted: RMS (red line) and 10 per. Mov. Avg. (RMS) (green line). The initial peak is very high, and the decay is very slow with significant oscillations.</p>

APPENDIX H – MATLAB CODE

```
%%%%%%%%%%%%%%%%%%%%%%%%%%%%%%%%%%%%%%%%%%%%%%%%%%%%%%%%%%  
%Dr. Ajay Mahajan and Gautham Ramesh  
%Department of MEEP, %Southern Illinois University  
%Date: October 2, 2008  
%Code written for Medtronic Paradigm Project - Paper2.m  
%”Neurosurgical Powered and Manual Torquing Instrument Performance  
%Comparison based on Tru-Trainer and Cadaver G-force Measurements”  
%Code to calculate the area under a curve  
%%%%%%%%%%%%%%%%%%%%%%%%%%%%%%%%%%%%%%%%%%%%%%%%%%%%%%%%%%  
clear;  
clc;  
CSV_FORMAT = 0;  
fig = 0;  
%Reading the Excel file  
SST1 = ['Z:\Work - Gautham\Gautham\Thesis\Documents\Medtronic Data\MERI  
- 08-27-08'];  
ST1_TEMP = ['\3Dx-TruTrainer-Manual-Modified'];  
ST1 = strcat(SST1,ST1_TEMP);  
ST2=['.csv'];  
  
if(CSV_FORMAT == 1)  
ST=strcat(ST1,ST2);  
D=[];  
fid=fopen(ST,'r');  
  
if (fid<0)  
error('file not found');  
else  
Line1=fgetl(fid);  
  
while(1)  
  
next_line=fgetl(fid);  
  
if(~ischar(next_line))  
break;  
end  
D=[D;str2num(next_line)];  
end  
  
fclose(fid);  
end % end of if(fid<0) block
```



```

else

%D] = xlsread(ST1);

[n,t] = xlsread(ST1,'3Dx-TruTrainer-Manual');
end
% end of if (CSV_FORMAT == 1) block

time=n(:,1);
rms=n(:,7);
m=length(time);
figure,plot(time,rms)

%h=(C(m,1)-C(1,1))/m;
%ar=(h/2)*(C(1,2)+C(n,2))+h*sum(C(2:n-1,2))

totalarea=0;
for i=1:m-1
a1=rms(i);
a2=rms(i+1);
h=abs(time(i+1)-time(i));
area=(a1+a2)*0.5*h;
totalarea=totalarea+area;
end
totalarea

%End of Code
%%%%%%%%%%%%%%%%%%%%%%%%%%%%%%%%%%%%%%%%%%%%%%%%%%%%%%%%%%%%%%%%%%%%%%%%%%

```

VITA

Graduate School
Southern Illinois University

Ganesh Gautham Aswapathi Ramesh

Date of Birth: May 18, 1981

Email Address: gautham.ar@gmail.com

Current Address:

1600 Logan Drive, Apt# 3, Carbondale, Illinois 62901

Permanent Address:

No. 303, Omkar Apartments,
12th Cross, 8th Main,
Malleswaram, Bangalore – 560003
Karnataka, India

Education:

People's Education Society Institute of Technology (P.E.S.I.T), Bangalore, India
Bachelor of Engineering, Mechanical Engineering, June 2003

Special Honors and Awards:

Graduate Teaching and Research Assistantships – Full tuition waiver with monthly stipend

Distinction Award, Department of ME, P.E.S.I.T, Bangalore, India

Cash Award from Board of Directors of Reserve Bank Employees Co-operative Bank

Thesis Title: Set Screw Break-Off Study in Spinal Neurosurgery

Major Professor: Dr. T. C. Chu